

The KNMI regional atmospheric climate model RACMO version 2.1

*E. van Meijgaard, L.H. van Uft,
W.J. van de Berg, F. C. Bosveld,
B.J.J.M. van den Hurk, G. Lenderink
and A.P. Siebesma*

De Bilt, 2008

PO Box 201
3730 AE De Bilt
Wilhelminalaan 10
De Bilt
The Netherlands
<http://www.knmi.nl>
Telephone +31(0)30-220 69 11
Telefax +31(0)30-221 04 07

Authors: Meijgaard, E. van
Ulft, L.H. van
Berg, W.J. van de
Bosveld, F.C.
Hurk, B.J.J.M. van den
Lenderink, G.
Siebesma, A.P.



The KNMI regional atmospheric climate model RACMO, version 2.1

Erik van Meijgaard¹⁾, Bert van Uft¹⁾, Willem Jan van de Berg²⁾, Fred C. Bosveld¹⁾, Bart van den Hurk¹⁾, Geert Lenderink¹⁾, A. Pier Siebesma¹⁾

¹⁾*Royal Netherlands Meteorological Institute (KNMI), PO Box 201, 3730 AE De Bilt, The Netherlands*

²⁾*Institute for Marine and Atmospheric Research, Utrecht University, PO Box 80.005, Princetonplein 5, 3584 CC Utrecht, The Netherlands*

KNMI

December 2008

1.	Introduction	1
2.	Summary of changes implemented in the previous version RACMO2.0	2
3.	Changes in the formulation of RACMO version 2.1	3
3.1	HIRLAM dynamical core	3
3.2	ECMWF physics	3
3.2.a	<i>Cumulus convection scheme</i>	4
3.2.b	<i>Prognostic cloud scheme</i>	6
3.2.c	<i>Land surface scheme</i>	6
3.2.d	<i>Charnock relation in the high wind speed regime</i>	9
3.2.e	<i>Diagnosis of 2-meter temperature under very stable conditions</i>	10
3.2.f	<i>Treatment of very thin snow pack</i>	12
4.	Surface Boundary Conditions	13
4.1	Surface Characteristics	13
4.2	Sea Surface Temperature and Sea Ice Extent	15
4.3	Lake Surface Temperature and Lake Ice Extent	16
5.	Dynamical Forcings	18
5.1	Single Column Models.....	18
5.2	RACMO output for Single Column Models	19
5.3	Time-height structure of dynamical forcings	22
5.4	Numerical accuracy	22
6.	Summary and Outlook	25
	Appendix A: Model Output	27
	Appendix A1: ASIMOF-GRIB formatted output.....	27
	Appendix A2: NetCDF formatted output.....	33
	Appendix A3: ASIMOF-GRIB to NetCDF converter	35
	Appendix B: Double precision float arithmetic	36
	Appendix C: Surface characteristics maps for Europe at 25 km resolution	37
	References	42

1. Introduction

In the last couple of years, since 2005, a next version of the KNMI regional climate model RACMO has been developed and applied in a number of projects. This version, hereafter referred to as RACMO2.1, constitutes an update of the RACMO2 cycle. The first version of this cycle, hereafter referred to as RACMO2.0, was built on the ECMWF physics package from cycle 23r4 embedded in the semi-Lagrangian (sL) dynamics kernel of the Numerical Weather Prediction (NWP) model HIRLAM5.0.6. This release of the ECMWF model also served as the basis for the ERA-40 project (White et al., 2004; <http://www.ecmwf.int/research/ifsdocs/>). The HIRLAM-5 project is comprehensively described in Undén et al. (2002). The performance of HIRLAM + ECMWF physics when operated in forecast mode is assessed and compared with the performance of an operational version of HIRLAM by de Bruijn and van Meijgaard, 2004. The modifications implemented in RACMO2.0 in order to improve its performance under present-day climate conditions have been extensively described by Lenderink et al., 2003. Version 2.0 has primarily been used in contribution to the EU-project PRUDENCE.

An important motivation to initiate the development of RACMO2.1 was provided by the findings that RACMO2.0 had a tendency to underestimate the occurrence of convective precipitation, in particular in Southern Europe and at the same time an overestimation of extreme values of daily precipitation amounts. The recent implementation in the ECMWF physics of a new trigger function for deep convection was expected to resolve this problem. Other considerations that led to the development effort included new releases of ECMWF physics, as recent as cycle 28r4, the introduction of a new data set to describe land surface characteristics (ECOCLIMAP), and the migration to the ECMWF high performance computational facility which made it necessary to include components of a more recent HIRLAM release (6.3.7).

So far, the baseline version of RACMO2.1 has been applied in multi-annual present-day and future climate calculations within the frameworks of EU-ENSEMBLES and the initial phase of the BSIK funded national program Climate changes Spatial Planning (CcSP). The same version is used in several other projects like multi-month simulations of the Hadley cell over the Pacific in contribution to a cloud radiation project under the umbrella of GEWEX-GCSS and an investigation of the sensitivity of summertime precipitation in the Netherlands to changes in coastal sea surface temperatures of the North Sea (Lenderink et al., 2008). Finally, a version of RACMO2.1 is extensively used in present-day climate calculations focusing on Antarctica and Greenland. For that purpose, the simple one-layer snow scheme of the baseline version was replaced with a four-layer snow scheme (Antarctica; Reijmer et al., 2005) - this adjustment was already made in RACMO2.0 - and a very advanced multi-layer snow-layer model including melting-refreezing conditions (only Greenland; Ettema et al., 2008).

The primary objective of this Technical Report is i) to document the changes of RACMO2.1 with respect to the preceding version, ii) to illustrate the effect of these changes by means of performing relatively short integrations on a small domain, and iii) to identify shortcomings in the model formulations that need to

be addressed in future work on model development. The report is not meant to provide a comprehensive technical description of the entire model. That type of information is already provided in technical documentation elsewhere describing the originating HIRLAM (Undén et al., 2001) and ECMWF (White, 2004) components.

In section 2, the report starts with briefly summarizing the alterations that were made in setting up the preceding version RACMO2.0, and the status of these changes in the current version. The central section 3 contains a description of additional modifications introduced in the current version, and briefly illustrates and discusses the effects of these changes to the model performance. Section 4 describes adjustments and new developments in the treatment of surface boundary conditions. The report closes with a brief outlook to the nearby future. For completeness we have included an appendix which contains a comprehensive overview of direct model output (DMO) produced by the model.

Finally, we refer the reader to section 5, where material is presented that is not related to the issues discussed in the preceding sections. Section 5 provides an introduction on dynamical forcings that may serve as driving information in operating local atmospheric models, e.g. Single Column Models (SCMs), Large Eddy Simulation models (LES). The information needed to compose the full set of dynamical forcings needed to drive a local atmospheric model is defined and identified from the rate equations governing the resolved-scale transport. The type of output that is collected in a dynamical forcings file is illustrated for the GABLS-3 case study. The content of section 5 is not of relevance to the performance of RACMO, yet it represents a crucial link between limited area models and local atmospheric models, because it provides a means to quantify information that can hardly be retrieved from observations, thereby allowing local atmospheric models to be operated in “observed” weather conditions.

2. Summary of changes implemented in the previous version RACMO2.0

The most important new features in setting up RACMO2.0 from the originating HIRLAM and ECMWF core included the following changes (see Lenderink et al., 2003):

1. Introduction of a revised relaxation scheme of prognostic variables in the lateral boundary zone of the model domain.
2. Reduction of resolved small-scale orographic variance by application of a Raymond filter in order to suppress the triggering of grid-scale disturbances by the dynamics solver. In addition, the RCM resolved orography is relaxed in the lateral boundary zone to match the coarser orography of the host model.
3. Reduction of the coefficient controlling the horizontal diffusion of specific humidity by a factor of 10.
4. Enhancement of soil model layers by a factor of 5/3 in order to allow the model to span a wider seasonal cycle in soil moisture amounts. Accompanying modifications affected the vegetation water stress function, and reduced the percolation speed by a factor of 10.

Modifications 1), 2) and 3) have been consolidated in RACMO 2.1 without change. Modification 4) has also been continued in version 2.1, however in a somewhat mitigated form, because it was felt that the changes in the soil hydraulic parameters had a tendency to overcompensate earlier problems of drying out. This aspect is discussed in more detail hereafter.

3. Changes in the formulation of RACMO version 2.1

Adjustments of the model formulation can be roughly distinguished into two categories, 1) the HIRLAM dynamical core, and 2) the ECMWF physics.

3.1 HIRLAM dynamical core

A number of components in the dynamical core of HIRLAM 6.3.7, absent in HIRLAM 5.0.6 have been incorporated in version 2.1. These involved the new implementation of MPI (Message Passing Interface) which made the model suitable for parallel processing on the IBM platforms of ECMWF computing facilities. Initially, asynchronous I/O, corresponding to another MPI related feature that was introduced in HIRLAM post 5.0.6, had not been transferred to RACMO. Because it was foreseen that the operation of the RCM would remain restricted to a relatively small number of processors, at most 64, being far less than the massive parallel environment used for the operation of the HIRLAM NWP, it was not considered worthwhile to make that effort. But at a later stage, in Spring 2008, we reconsidered this point and ported the asynchronous I/O feature into RACMO to reduce elapsed times of RACMO-Greenland@11 km simulations on four nodes at ECMWF HPC or the NCF/Huygens platform.

Concerning the treatment of dynamical processes, HIRLAM 6.3.3 was found very similar to HIRLAM 5.0.6, hence the number of updates in the dynamics formulation remained very limited. The only significant update involved a more advanced treatment of semi-Lagrangian propagation of the temperature field in the vicinity of orography. Application of this technique, referred to as the Ritchie-Tanguay (R-T) interpolation, was found to reduce noise and prevent the occurrence of “grid point storms” in the HIRLAM forecast model (Eerola, 2004). In addition, it results in smoother precipitation fields in orographic regions. This is illustrated in Figure 1, where precipitation amounts of a one-month integration with (left panel) and without (right panel) R-T interpolation are compared for a small test domain. The precipitation over mountainous regions in the interiors of the model domain (Alps, Apennines, Pyrenees, Balkan countries) is much smoother in the integration with R-T interpolation. In the lateral boundary zone (width 16 points) the differences are obscured by the process of relaxation.

3.2 ECMWF physics

Adjustments to the physics packages included quite a few modifications, some of them major with significant impacts on the model behaviour, some of them minor with hardly noticeable impact on the model performance except for one or two meteorological parameters, some of them only meant to extend or improve diagnostics. The changes are discussed hereafter in that order.

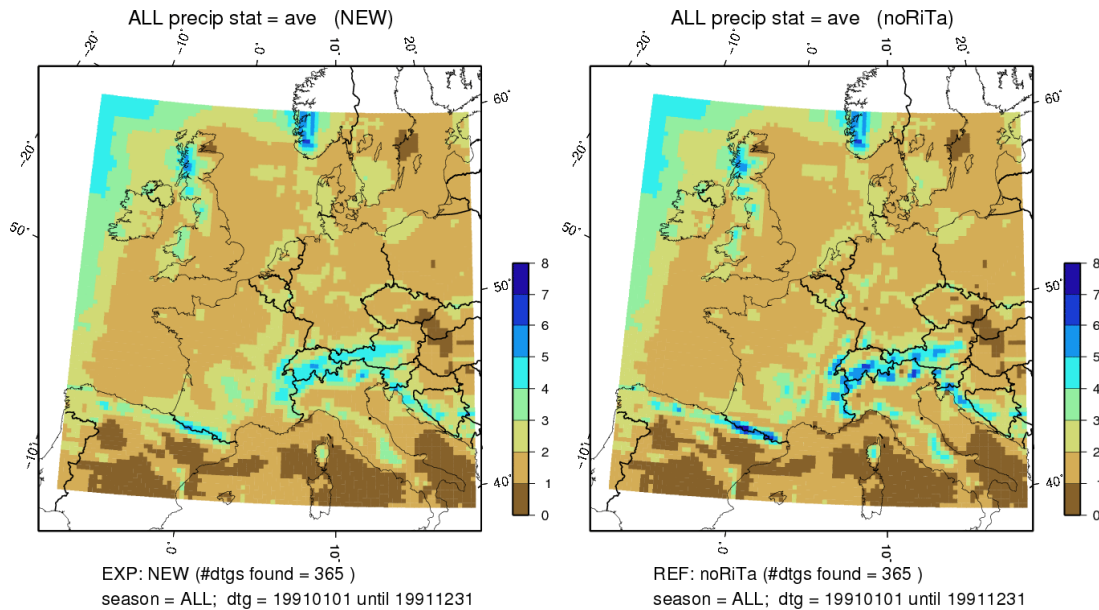


Figure 1: effect of Ritchie-Tanguay (R-T) interpolation of temperature on precipitation. Left panel shows precipitation from a 1-month integration including R-T interpolation, right panel shows precipitation from an equivalent integration excluding R-T interpolation.

3.2.a Cumulus convection scheme

The most extensive change, also concerning computer code, involved the substitution of the entire cumulus convection scheme by a more recent version from ECMWF cycle 28r1. The important new feature of the updated scheme consists of a reformulation of the triggering of shallow and deep convection over land proposed by Jakob and Siebesma (2003). The cumulus convection scheme, including the triggering function, is extensively described in the Integrated Forecast System (IFS) documentation of cycles 28r1 and 31r1. Test runs with a preliminary version of RACMO2.1 resulted in a considerable overestimation of precipitation amounts compared to version 2.0, and also indicated that the new version had a strong tendency to produce light, but continuous precipitation. This outcome led us to implement two further adjustments. In the IFS version shallow convection can be overruled by deep convection. This is prevented by an adjustment in RACMO2.1 which forces deep convection to be ignored once shallow convection is triggered. The effect of this change is modest, nevertheless it is retained for reasons of consistency. The second adjustment is related to the setting of a threshold for minimum convective (geopotential) depth, referred to as Z_{dnoprc} that is required for the onset of precipitation production. In earlier IFS cycles, prior to 28r1, Z_{dnoprc} was set to $1.5 \cdot 10^4 \text{ m}^2 \text{ s}^{-2}$ over sea. Over land, the value was set to $3.0 \cdot 10^4 \text{ m}^2 \text{ s}^{-2}$ in general, but was enhanced to the size of the convective depth of the updraft in case the updraft temperature at cloud top was above -13°C . Eventually, values over land were clipped between $3.0 \cdot 10^4$ and $5.0 \cdot 10^4 \text{ m}^2 \text{ s}^{-2}$, which seem sensible values. Remarkably, in cycle 28r1 its value was found set to $0. \text{ m}^2 \text{ s}^{-2}$ in any case, but neither this setting nor the motivation for the change are mentioned in any of the IFS documentations. The zero setting might explain the continuous production of precipitation. In RACMO2.1, we have reinstalled the

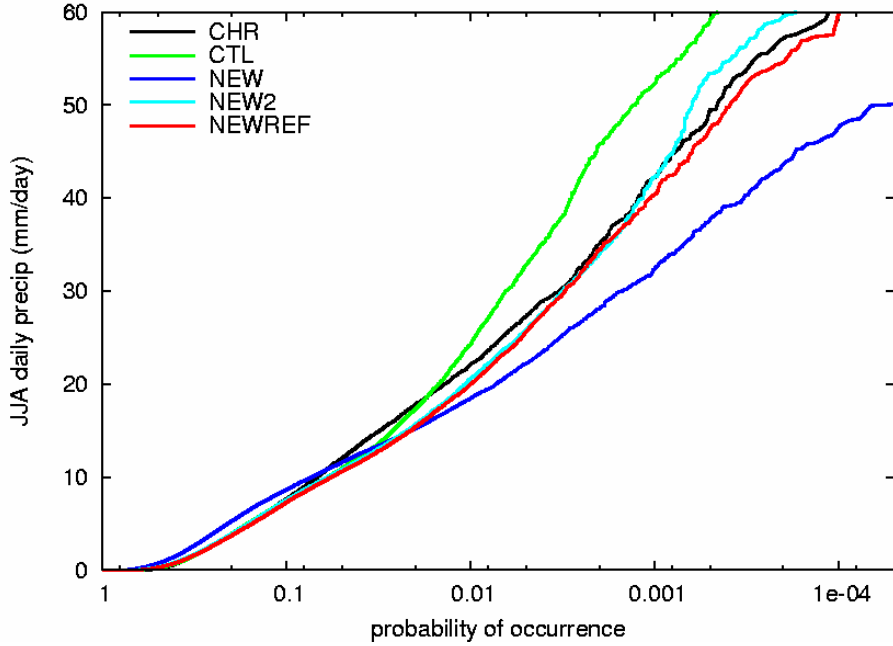


Figure 2: Probability of exceedance for daily precipitation in summertime (JJA; 1991-1995) on sub-catchment scale across the German portion of the Rhine catchment. Observations are from Commissie Hydrologie Rijn (CHR). Simulations are from RACMO2.0 (CTL), RACMO2.1 (NEWREF), and two preliminary versions of RACMO2.1, one with the threshold parameter $Z_{dnoprc} = 0$ (NEW ; this is the reference setting in ECMWF physics), and one with the parameter set to value between 1.5 and $3.0 \cdot 10^4 \text{ m}^2\text{s}^{-2}$ (NEW2).

previous formulation, but with reduced values over land, varying between $1.5 \cdot 10^4$ and $3.0 \cdot 10^4 \text{ m}^2\text{s}^{-2}$. The restoring of physically sound values into Z_{dnoprc} has serious impacts on the model outcome. It reduces the mean precipitation, it also reduces the tendency to produce continuous rainfall, and it yields a better representation of extreme events of daily precipitation in e.g. the Rhine catchment area as is illustrated in Figure 2.

This provided us the primary motivation to reinstall an older formulation of Z_{dnoprc} in RACMO2.1, but with slightly modified numbers. However, in a recent study (Roebeling and van Meijgaard, 2008) focusing on the evaluation of RACMO predicted liquid water path with observations inferred from MSG-SEVIRI it is found that the model predicted daytime mean liquid water path, obtained during a summer season and averaged over a large domain, significantly overestimates the observed liquid water path by 55% to 80%, dependent on model resolution. Interestingly, the overestimation is found reduced to about 30%, when Z_{dnoprc} is set back to 0. This points to a strong sensitivity in both precipitation and cloud parameters to variations in this single parameter, probably much more than is desirable. It also suggests that there are compensating errors, since an improvement in representing precipitation is achieved at the expense of performance in representing columnar liquid water amounts.

3.2.b Prognostic cloud scheme

To begin with, the entire prognostic cloud scheme from IFS cycle 25r4 was substituted for the version used in cy23r4. This was primarily done in view of the recoded numerics which had considerably improved the transparency of the code. Once the recoded version was introduced into the operational ECMWF-IFS system it appeared that the new numerics, though unintentionally, also had an impact on the performance of the scheme in a meteorological sense, in particular it was found that precipitation amounts had increased.

A major modification to the prognostic cloud scheme in RACMO2.1 concerns the formation of precipitation, specifically the partitioning of cloud liquid water and cloud ice into rain and snow. Model integrations over Antarctica and, later, Greenland showed that the model generated unrealistically large amounts of rain, while total precipitation was produced in the right order of magnitude. This could be traced back to the treatment of autoconversion in mixed clouds. The ECMWF model employs a simple temperature dependent prescription for the partitioning of cloud condensate into the liquid and the solid phase:

$$\alpha = 0 \text{ for } T \leq T_{ice}; \quad \alpha = \left(\frac{T - T_{ice}}{T_0 - T_{ice}} \right)^2 \text{ for } T_{ice} < T \leq T_0; \quad \alpha = 1 \text{ for } T \geq T_0,$$

where α denotes the fraction of liquid water and T_{ice} and T_0 represent the temperatures 250.16°K and 273.16°K, respectively. The same partitioning is used throughout the model and also applies to the fractioning of rain and snow when formed in mixed phase clouds, implying that the autoconversion of condensate into precipitation in mixed phase clouds occurs without phase changes. We consider the latter assumption inadequate, in fact there is substantial evidence that in mixed phase clouds precipitation will develop as solid only (Rogers and Yau, 1989). We have adjusted the conversion parameterization in such a way that all precipitation formed in mixed phase clouds will start as solid if the temperature is below -1°C. (In later runs focussing on Greenland (Ettema et al., 2008) this threshold value is reduced to -7°C). The accompanying latent heat release is brought into account to the temperature tendency, but since phase changes occur only from the liquid to the solid state, these contributions are relatively small. Of course, solid precipitation can still reach the surface as rain, but that requires that precipitation falls through a melting layer. The effect of this modification, derived from two one-year integrations over Antarctica, is shown in Figure 3.

3.2.c Land surface scheme

The drastic changes in the treatment of soil moisture that were implemented in RACMO2.0 (see section 2) have been retained in a mitigated form. The reason is that the parameter setting of version 2.0 with its very thick layers and non-linear water stress function hardly allows soil drying out to occur. Hence, in RACMO2.1 the soil layers remain thicker than in the original ECMWF code but shallower than in RACMO 2.0. Layer depths have been set to (0.07, 0.27, 1.00, 2.60), resulting in a total soil depth of 3.94 m. With respect to the original ECMWF code the thicknesses of all layers but the top layer have been enhanced by roughly a factor 4/3, whereas the top layer remained unchanged to retain a similar temperature response of the soil to the diurnal cycle. The root fraction

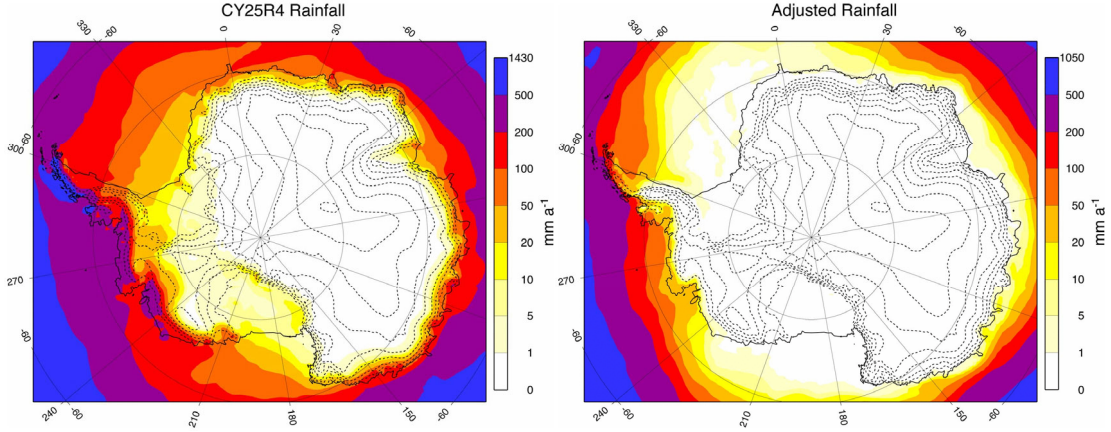


Figure 3: Rainfall produced by 1-year runs with RACMO over Antarctica with the original cy25r4 prognostic cloud scheme (left panel) and the modified scheme containing adjustments in the formation of rain and snow in mixed phase clouds using a threshold of -1°C (right panel).

formulation is changed correspondingly in such a way that the root fraction density as a function of the soil layer number remains invariant.

Similarly, the water stress function $f(\theta)$, being a reciprocal factor in the resistance formulation determined by vegetation, retained its non-linear shape as introduced in version 2.0 (but in a mitigated form):

$$f(\theta) = \alpha((\theta - \theta_{pwp})/(\theta_{cap} - \theta_{pwp}))^p + (1 - \alpha)(1 - (1 - (\theta - \theta_{pwp})/(\theta_{cap} - \theta_{pwp}))^q),$$

where θ , θ_{pwp} and θ_{cap} denote the actual soil moisture content of the top layer, the soil moisture at permanent wilting point and the soil moisture at field capacity, respectively. The functional dependence is applied in the range $\theta_{pwp} \leq \theta \leq \theta_{cap}$. For $\theta < \theta_{pwp}$ and $\theta > \theta_{cap}$, $f(\theta)$ is set to 0 or 1, respectively. The exponents p and q determine the level of non-linearity, the coefficient α determines the cross-over point with the linear form. In RACMO2.0 the values of α , p and q had been set to 0.7, 0.3 and 0.3, respectively. In RACMO2.1 the non-linearity is somewhat mitigated by choosing $p = 0.5$, the first term is also given somewhat more weight by setting $\alpha = 0.75$. In the original ECWMF formulation (cycle 23r4), but also later cycles like 31r1, the shape is linear ($\alpha = 1.0$, $p = 1.0$, q is not relevant).

The nonlinear expressions of $f(\theta)$ are chosen such that evaporation is reduced for soil moisture near field capacity, while a higher evaporation is supported for intermediate values of soil moisture. The various expressions of $f(\theta)$ are shown in Figure 4.

A corresponding change involves the setting of the percolation speed at which soil water infiltrates to deeper soil layers. While in version 2.0 it was set to 10% of the original value, in version 2.1 its adjustment is now reduced to 33% of the original value ($4.5 \cdot 10^{-6} \text{ms}^{-1}$). This change is applied to remain consistent with the previous two alterations, though its effect is very modest.

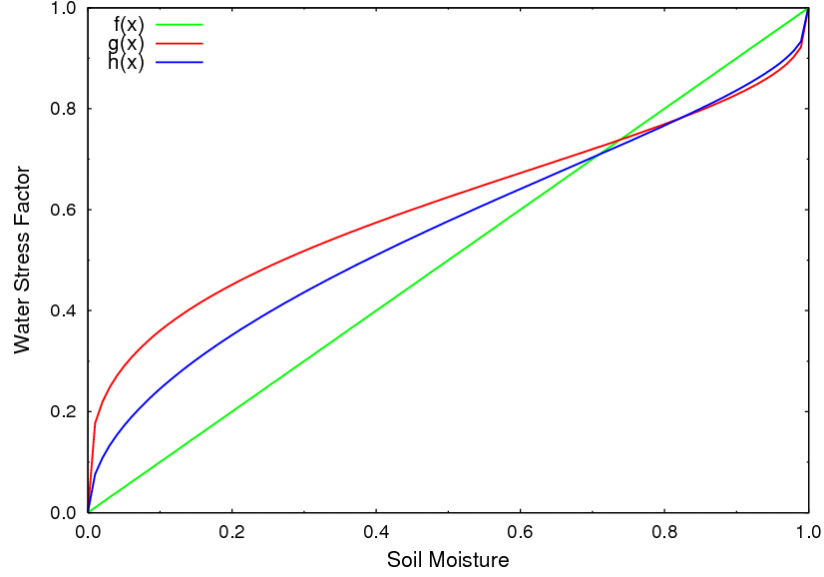


Figure 4: Various functional forms of the water stress function. $f(x)$: original formulation applied in ECMWF cycles, $g(x)$: formulation employed in RACMO2.0, $h(x)$: formulation employed in RACMO2.1.

In addition to the above changes in the land surface scheme, which can be regarded as continuations of changes already made in version 2.0, one further adjustment and one extension has been made to the land surface scheme.

The adjustment involves the setting of the canopy resistance of low vegetation. It has been increased from 0. to 0.2 $\text{ms}^{-1}\text{kgkg}^{-1}$ in order to limit the evaporation in the condition of high vapour deficit. The canopy resistance of high vegetation kept its value of 0.3 $\text{ms}^{-1}\text{kgkg}^{-1}$.

The extension includes the introduction of a surface runoff scheme controlled by orographic variance. The scheme, originally proposed by Dümenil and Todini (1992), was already employed in ECHAM3 and 4, and in RACMO1. It is formally expressed as

$$R_R = Q - \rho_w (W_{S_{\max}} - W_S) + \rho_w W_{S_{\max}} \left\{ \max\left(0, \left(1 - \frac{W_S}{W_{S_{\max}}}\right)^{\frac{1}{1+b}} - \frac{Q}{(1+b)W_{S_{\max}}}\right)\right\}^{1+b},$$

with R_R and Q respectively denoting the surface runoff and sum of throughfalling rain (i.e. rainfall diminished by the intercepted amount) and snow melt. The units of R_R and Q in this equation are kgm^{-2} . W_S and $W_{S_{\max}}$ represent the soil moisture and maximum soil moisture amount in the uppermost SRDEP meters. Here, SRDEP is set to 0.5 m. ρ_w is the density of water (1000 kgm^{-3}), and the structure parameter b is a measure of the typical steepness of the terrain in the designated grid box:

$$b = \frac{\sigma_h - \sigma_0}{\sigma_h + \sigma_{\max}},$$

where σ_h is the standard deviation of the terrain height in meters, and σ_0 and σ_{\max} are a prescribed minimum and maximum value of the standard deviation. Here, $\sigma_0 = 100\text{m}$ and $\sigma_{\max} = 1000\text{m}$. Furthermore, b is constrained by b_{\min} and b_{\max} with $b_{\min} = 0.01$ and $b_{\max} = 0.5$ ($\sigma_h \cong \sigma_{\max}$).

3.2.d Charnock relation in the high wind speed regime

In a model comparison study by De Bruijn and van Meijgaard (2004), observed values of 10 meter wind speed over sea in the high wind speed regime were found underestimated by the model. To improve the model representation we have altered the surface roughness length z_{0m} over sea in the high wind speed regime by slightly reformulating the Charnock relation according to

$$z_{0m} = \alpha_{Ch} \frac{u_*^2}{g} \longrightarrow \alpha_{Ch} \frac{u_{\text{lim}}^2 (1 - \exp(-\frac{u_*}{u_{\text{lim}}}))^2}{g}$$

Here, u_* denotes the friction velocity and u_{lim} a threshold velocity value beyond which the revised Charnock relation starts to deviate from the original expression. Here we have set u_{lim} to 1 ms^{-1} . The Charnock coefficient α_{Ch} remains set to 0.018 ; g denotes the gravitational constant. The new expression for z_{0m} becomes constant at high frictional velocity, and hence yields a momentum transfer coefficient C_m (or drag coefficient C_d) which in the limit of high wind speed takes the form

$$C_m = \frac{\kappa^2}{\log^2\left(\frac{z_{Nlev} + z_{0m}}{z_{0m}}\right)},$$

where z_{Nlev} is the lowest model level ($\sim 10\text{m}$) and κ is the Von Kármán constant. u_* is computed from the wind speed and the transfer coefficient C_m as

$$u_* = C_m^{1/2} (u^2 + v^2 + w_*^2)^{1/2},$$

where u , v denote the horizontal wind speeds at the lowest model level and w_* the free convection velocity scale. Adopting the new expression of the Charnock relation results in a constant z_{0m} and, hence, constant C_m at high wind speed. The latter behaviour is confirmed by observations (Donelan et al., 2004, their Fig. 2; Zhang et al. 2006, their Fig. 1). Frictional velocity grows linearly with the wind speed, which implies a reduction in growth compared to the original formulation. The modification eventually results in a slight increase of the diagnosed 10 meter wind speeds. Adopting the current settings, 10 meter wind speeds are found increased by about 5 to 10% in the regime above 20ms^{-1} , otherwise the effect is negligible. The relative impact of the new formulation is shown in Figure 5, where the frequency distributions of daily maximum 10 min wind speed values for all sea points of the test area SNS25 of a 5-year period are compared. Also the exceedance levels of maximum 10 meter wind speed values indicate a small but well defined shift to somewhat higher wind speed values when comparing the new with the original formulation.

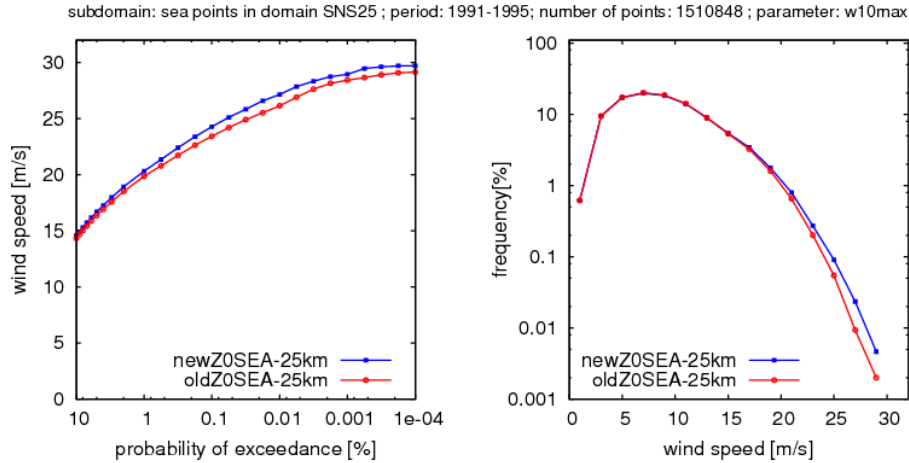


Figure 5: Effect of the reformulation of the Charnock relation in the high wind regime over sea to the statistics of the 10-meter wind speed (newZ0SEA: adjusted formulation; oldZ0SEA original formulation).

3.2.e Diagnosis of 2-meter temperature under very stable conditions

When conditions in the model boundary layer become very stable the diagnosed 2-meter temperature may exhibit strange behaviour like shown in Figure 6 (blue curve). Although this problem does not affect the model evolution as the diagnosed 2-meter temperature does not feed back on any of the model prognostic variables this type of behaviour is undesired since it produces a positive bias in the daily mean 2-meter temperature and the mean daily 2-meter minimum temperature. In particular, it may result in an underestimation of the

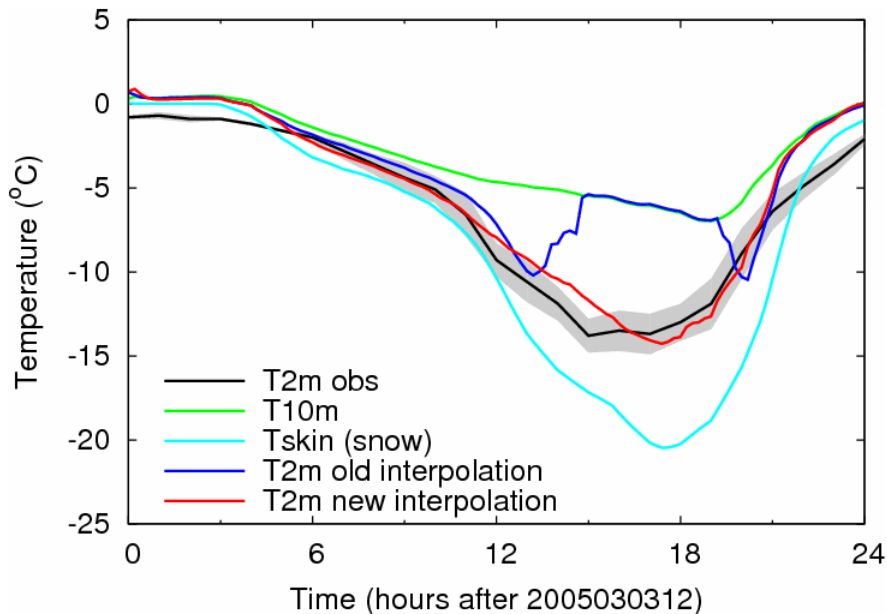


Figure 6: Time series of 2 meter temperature observed (black curve) at Cabauw during the extremely cold night of 4 March 2005. Also shown are modelled time series inferred from routinely made forecasts with RACMO@55 km. See text for details

occurrence rate of low 2-meter temperatures, where “low” should be interpreted relative to location and time of the year.

In the model, the 2-meter temperature is diagnosed for the dominant tile according to a formula expressed in Eq. 3.69 in the IFS documentation of CY23r4 (or Eq. 3.93 in the documentation of CY31r1):

$$s_2 = s_{surf} + (s_l - s_{surf})\alpha$$

with s representing the dry static energy, and the indices 2, *surf* and l denoting the 2m level, the surface and a near-surface reference level, here represented by the lowest atmospheric model level. The temperature T is inferred from the dry static energy according to:

$$s = c_p T + gz,$$

where z is the height relative to the surface, and c_p the specific heat of moist air.

Relevant for the problem under consideration is the interpolation factor α which is expressed as

$$\alpha = \frac{\log\left(\frac{z_2 + z_{0mWMO}}{z_{0hWMO}}\right) - \Psi_m\left(\frac{z_2 + z_{0mWMO}}{L}\right) + \Psi_m\left(\frac{z_{0hWMO}}{L}\right)}{\log\left(\frac{z_l + z_{0mWMO}}{z_{0hWMO}}\right) - \Psi_m\left(\frac{z_l + z_{0mWMO}}{L}\right) + \Psi_m\left(\frac{z_{0hWMO}}{L}\right)},$$

where $z_2 = 2\text{m}$, z_l is the height of the lowest model level (about 10 m), and the WMO labelled roughness lengths are prescribed from the model roughness lengths according to $z_{0mWMO} = \min(z_{0m}, 0.03)$, and $z_{0hWMO} = 0.003$ if $z_{0m} > 0.03$, otherwise $z_{0hWMO} = z_{0h}$. The Obukhov length L represents the stability parameter and Ψ_m denotes a universal profile stability function.

The reason for the bumps in the time series of the 2-meter temperature is the Obukhov length approaching zero for very stable conditions. In that situation, the ratio z/L becomes very large, which results in unrealistic profile shapes with standard stability functions. In the original code this is resolved by maximizing z/L to 5, which is achieved by defining the heights z_l and z_2 as z_h in the expression for α so as to satisfy $z_h/L = 5$. This implies that the interpolation factor α becomes identically 1 once the Obukhov length falls below $(z_2 + z_{0mWMO})/5$, which results in a 2-meter temperature equal to the temperature of the lowest model layer. This procedure is based on the assumption that under conditions with $L < 0.4$ m all temperature gradient in the lowest model layer is concentrated between 0 and 2 meters, or less. This is not a realistic assumption as is shown in Figure 7.

Imposing a maximum number for z/L at much higher values, e.g. 50 or 500, does not resolve the problem. Ultimately, L becomes so small that z/L exceeds the threshold, and the bumpy behaviour becomes manifest. Therefore we have implemented an alternative approach for the diagnosis of 2-meter temperature

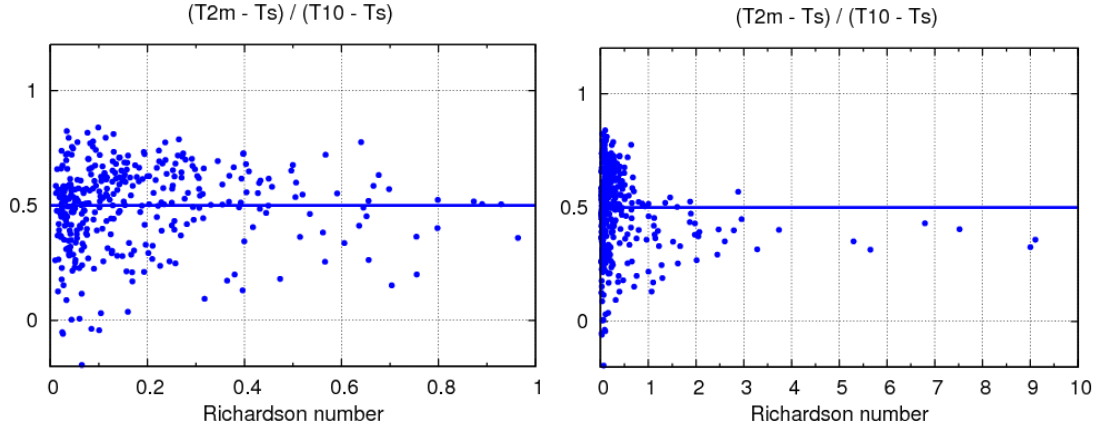


Figure 7: Observations of the near-surface temperature fraction as a function of Richardson number. Inferred from measurements taken at Cabauw in the winter of 2004/2005.

and (relative) humidity under stable conditions. Instead of imposing a maximum value to z/L , we replaced the interpolation factor by

$$\alpha' = \alpha(1 - f) + \lambda f,$$

with

$$f = \frac{2}{\pi} \arctan(\gamma z/L),$$

where the parameters γ and λ are set to 0.3 and 0.5, respectively. λ determines the limit for very stable conditions, while γ controls how fast this limit behaviour is approached. The effect of this substitution is illustrated in Figure 6 which shows the evolution of the modelled and observed 2-meter temperature during a night in March 2005 when very low temperatures were recorded at Cabauw favoured by extremely stable conditions. Evidently, the new approach results in a continuous evolution of 2-meter temperature which at its minimum is half way between the skin temperature and the temperature of the lowest model layer at 10m. In the reference treatment the 2-meter temperature jumps to the temperature of the lowest model layer indicating that the ratio z_{2m}/L is larger than 5 in that regime.

3.2.f Treatment of very thin snow pack

Analysis of snowpack temperature (TSN) revealed possible run-away behaviour in the case of very thin snowpack. At some occasions TSN was found to take negative temperatures resulting in NaN values for variables based on TSN and inevitably ending in a model crash. The problem seemed to occur mostly under the condition of very low snow mass and at the same time persistent snow mass increment due to snowfall. Slow run away behaviour could trigger a rapidly magnifying oscillation of TSN between the melting point and an absurdly low temperature. Reduction of the model time step size seems part of the solution. The full remedy includes three modifications:

- Routine `vdfourter.F90` is re-introduced between `callpar.F90` and `vdmain.F90`, and `INVDF` is set to 2, enforcing that the `vd`-routines are passed twice during a model time step. It establishes the smaller time step where it is needed, namely in the surface flux computation. This removes the oscillations!
- Constant `RFRSMALL` (set in `susoil.F90`) is increased by a factor of 1000. This seems also consistent with the IFS-documentation where it is stated that a snow tile fraction (tiles 5+7) of 0.1% should be considered as the threshold. The enhanced value of `RFRSMALL` matches this threshold.
- When the snow-tile fraction is smaller than the threshold (`RFRSMALL`) the corresponding very small but non-zero snow mass (`SNS`) is removed and included as frozen soil water in the upper soil layer (`WSA1`).

The first bullet is now the model default, the second and third bullet are controlled by the compiler directive `EVM_VERYTHINSNOWPACK`. The impact of the changed model formulation is seen in Figure 8 which shows the 6-hourly resolved domain lowest snow pack temperature of the RACMO2-MIROC@50km integration for January 1954. Minimum TSN in the "stabilized TSN" result is no longer running away, yet it is still not entirely smooth. This comes from grid points where snow pack fractions just above the threshold are maintained for a somewhat longer time permitting TSN to drift slowly away. Once the snow tile fraction drops below the threshold or becomes thicker as a result of intensifying snow fall the loose behaviour of TSN disappears.

4. Surface Boundary Conditions

4.1 Surface Characteristics

Application of RACMO2 requires the specification of a number of surface properties. When these properties have spatial structures their contents are prescribed to the model as two-dimensional fields. Some of these properties are

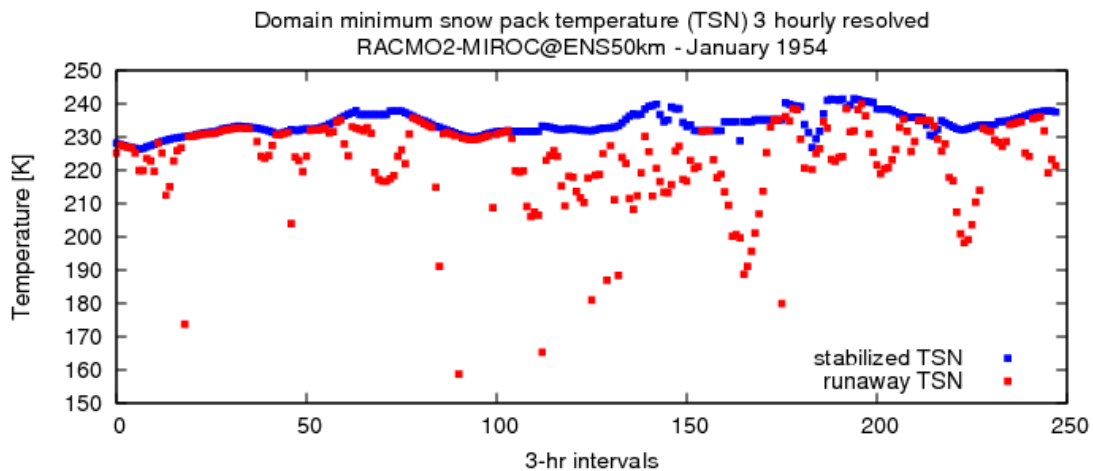


Figure 8: 3-hour resolved domain minimum snow pack temperatures taken from a one-month RACMO integration. Shown are values before (runaway TSN) and after (stabilized TSN) installing the remedy of controlling very thins snowpack conditions.

fixed in time, like e.g. surface orography and land-sea mask. Some of them have a seasonal cycle like e.g. roughness length of vegetation. Both types of properties are loosely called climate fields and are collected in what is called climate files. It is always assumed that climate fields are fixed in time or have a fixed seasonal cycle, and do not respond to the model evolution. Whenever a prescribed surface field, like e.g. sea surface temperature or sea-ice extent, deviates from this description it does not fall into the category of climate fields. RACMO2.1 uses 18 climate fields to specify the surface characteristics (see Table 1).

Climate fields are prepared in a procedure referred to as climate file generation. This is a stand alone procedure which, after specification of the model domain and horizontal resolution, needs to be applied one time in setting up the experiment. It produces twelve monthly climate files in GRIB format, each containing the climate fields listed in Table 1. The climate fields are based on information from different origins available at different resolution and different projection. Essentially, topography related parameters, like `phis` and its higher order sub-grid scale moments like `hstd`, `hsdfor`, `gamma`, `theta` and `sigma` are based on the terrain elevation data set GTOPO30 (<http://edc.usgs.gov/products/elevation/gtopo30/gtopo30.html>). For domains covering Antarctica and Greenland more accurate elevation data sets are available. Most of the other surface parameters (`lsm`, `lake`, `alb`, `tvh`, `cvh`, `tv1`, `cv1`, `urb`, `z0v`) are based on the data set ECOCLIMAP, version 1 (Champeaux et al., 2003).

The roughness lengths of `z0m` and `z0h` are prepared following the procedure

Table 4-1: Specification of climate fields used in integrations with RACMO2.1. The last column indicates whether fields have a seasonal cycle (S) or their values are fixed (F). In appendix C maps are shown for fields of which the number is printed in a grey cell.

	Climate field	Abbr.	Required by RACMO2.1 component	F/S
1	Surface Orography	<code>phis</code>	Entire model	F
2	Land-Sea Mask	<code>lsm</code>	Entire model	F
3	Background Surface Albedo	<code>albf</code>	Radiation	F
4	Roughness Length for Momentum	<code>z0m</code>	Interactions with the surface over land	S
5	Roughness Length for Heat	<code>z0h</code>	Interactions with the surface over land	S
6	Roughness Length of vegetation	<code>z0v</code>	Specification of <code>z0m</code> and <code>z0h</code>	S
7	Urbanisation	<code>urb</code>	Specification of <code>z0m</code> and <code>z0h</code>	F
8	Type of High Vegetation	<code>tvh</code>	Land surface parameterization	F
9	Fraction of High Vegetation	<code>cvh</code>	Land surface parameterization	F
10	Type of Low Vegetation	<code>tv1</code>	Land surface parameterization	F
11	Fraction of Low Vegetation	<code>cv1</code>	Land surface parameterization	F
12	Standard Deviation of Subgrid-scale Height	<code>hstd</code>	Surface runoff; subgrid-scale orographic drag	F
13	Filtered Standard Deviation of Subgrid-scale Height	<code>hsdfor</code>	Specification of <code>z0m</code> and <code>z0h</code>	F
14	Anisotropy of Orography	<code>gamma</code>	Subgrid-scale orographic drag	F
15	Orientation of Orography	<code>theta</code>	Subgrid-scale orographic drag	F
16	Mean Slope of Orography	<code>sigma</code>	Subgrid-scale orographic drag	F
17	Lake Mask	<code>lake</code>	Surface parameterization	F
18	Land Ice	<code>landice</code>	Land surface parameterization (only used in RACMO-Greenland run)	F

outlined in the IFS documentation, paragraph 9.5. They form a blend of three sources: subgrid-scale orography (`hstd`), vegetation (`z0v`) and urbanisation (`urb`). According to the IFS documentation, the contribution from subgrid-scale orography was first derived from a US-Navy data set. However, this data set is no longer useful at current model resolutions, because it is configured at a mesh of $1/6^\circ$, which makes that contributions from the standard deviation of the resolved part vanish for model resolutions finer than about 18 km. To overcome this problem we have replaced the sum of resolved and subgrid-scale variance as derived from the US-Navy data set by the standard deviation (`hsdfor`) of subgrid-scale orography in the spectral range between 2 and 20 km (Beljaars et al., 2004)

$$\text{hsdfor} \leftarrow 4 \cdot (\sqrt{\sigma_r^2 + \sigma_s^2}) \quad ; \quad \text{slope} \leftarrow S_i$$

where the standard deviations σ_r and σ_s , respectively referring to the component that is resolved by 30'x30' US Navy data and the component that is subgrid-scale to the 30'x30' data, together with the slope parameter S_i were computed according to the outline in the IFS documentation. In all versions of RACMO2, the calculation of `z0m` and `z0h` is part of the climate file generation.

4.2 Sea Surface Temperature and Sea Ice Extent

The regional model requires two characterizing fields to specify the surface boundary conditions over sea (SSBC), namely sea surface temperature (SST) and sea ice extent (CI). Since both parameters vary strongly in time they can not be prescribed as a climate field. In general, SST and CI are adopted from the same source that provides the atmospheric information used to satisfy the lateral boundary conditions, i.e NWP operational analyses or re-analyses, or a climate model. Since the SSBCs are the only external information that directly affects the interior of the RCM-domain during integration, projection from the host grid to the RCM grid must be carried out carefully. Also, since the host grid is much coarser than the receiving RCM grid the projection involves disaggregation of information implying the introduction of additional degrees of freedom that can not be determined. In particular, in the vicinity of land-sea transitions or near the edges of sea ice coverage, the specifics of the interpolation of projection can make a difference.

In the current implementation the projection of a coarse-gridded SST field on a finer grid is based on a simple bi-linear interpolation scheme. The SST at a RACMO sea grid point is calculated from the host-SSTs at the four adjacent host grid boxes, provided these are sea points. Complications arise when one or more of the adjacent host grid boxes are land points lacking valid SST information. To deal with all possible combinations that can occur, and also do occur, we have set up a scheme of rules that are subsequently applied in order to infer a plausible SST value at the designated RCM sea grid point. Consider a 4x4 portion of the

A	B	C	D
E	1	2	F
G	3	4	H
I	J	K	L

host grid with the four grid points 1-4 in the inner square surrounding the RCM sea grid point, and the 12 gridpoints A-L in the perimeter representing next nearest grid points:

First, missing SST values, if any, in the inner square are supplied with SST information from one or more of the remaining host grid boxes in the perimeter. Once SST values are loaded to all inner square grid points, the SST at the RCM grid point is determined from bi-linear interpolation. To import SST information into an inner square grid point where SST information is lacking, the following chain of rules is applied in the indicated order. Suppose that SST in point 4 is missing.

1. apply linear interpolation to at least one of the pairs 3-H and 2-K. If both succeed combine them with equal weight, if both fail go to next step.
2. span a plane with SST values from 1,2 and 3, if any of them is missing goto next step
3. apply linear extrapolation to at least one of the pairs G-3 and C-2. If both succeed combine them with equal weight, if both fail go to next step.
4. make an average over the non-missing values of the eight surrounding grid points 1,2,F,3,H,J,K,L. If that fails go to the final step
5. make an average over all non-missing values in 4x4 grid area. If that fails the SST is loaded from a backup climate field.

In general, the above scheme is capable of deriving plausible SST values on the RCM grid from coarse-grained host information. Over open sea and oceans the scheme straightforwardly applies a bi-linear interpolation scheme to the host field. In the vicinity of land-sea transitions the scheme imposes a linear gradient in SST at RCM sea boxes that are only bounded by host sea boxes on one side. This feature is owing to rule number 3 which explicitly prescribes SST through linear extrapolation partly based on values from outside the inner square. Given the fact that most seas becomes shallower near the coast with sea surface temperatures more rapidly responding to atmospheric forcings, the linear result is likely a more realistic result than assuming an SST continuation based on a average value of nearest and next nearest host grid boxes.

An example is contained in Figure 9 which shows the projection of the coarse-grained SST to a 2.5 km resolution RACMO domain.

The above scheme is also applied to sea ice extent (CI), with land and open sea taking the role of land in the SST interpolation. After projection of the host CI to the RCM grid, CI-values are constrained to values between 0 and 1.

4.3 Lake Surface Temperature and Lake Ice Extent

Failing of the above scheme to yield a plausible SST-value at the RCM point under consideration implies that the RCM point is entirely isolated from the host grid and is most probably representing a lake point resolved in the finer RCM horizontal grid, but not found in the coarse host grid. To load lake surface temperature (LST) we apply a very simple on-line algorithm which links LST to deeper soil temperature fields of lake-shore land points. The procedure is as follows. First an algorithm is applied that identifies lakes and labels them with a sequential number. Different lakes are separated by land points, the minimum size of a lake is one grid box, and lakes cannot border to the outermost line of

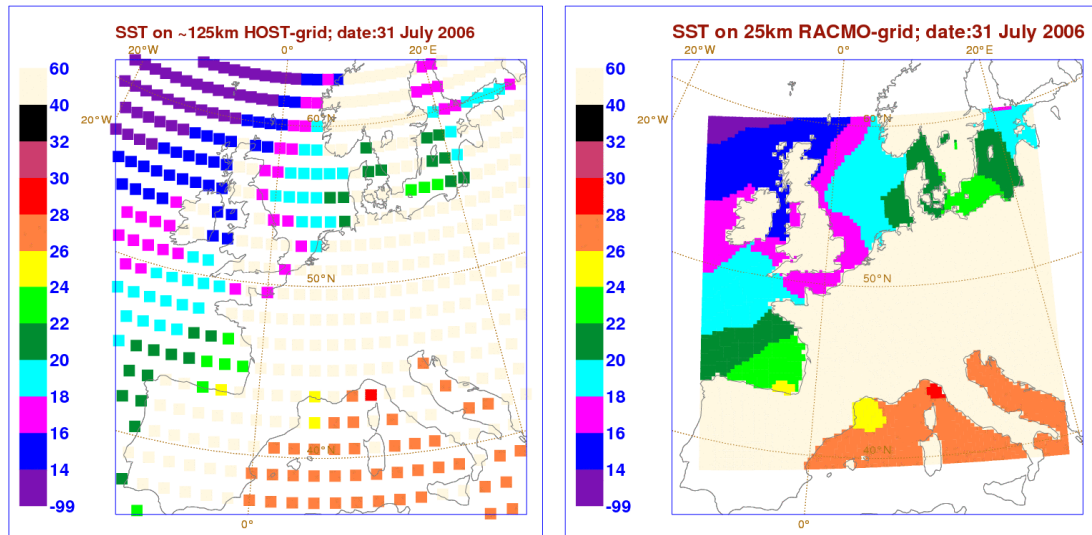


Figure 9: Projection of coarse-grained SST information (in this case obtained from a MIROC3.2 hires run at 1.25° resolution) to the RACMO grid at 25 resolution.

lateral grid points. The latter implies that all points that are connected to the outmost boundary points of the domain are regarded as sea points (or sea ice points). Once a lake is designated, the lake shore land points corresponding to the lake are identified. The LST-scheme then proceeds by diagnostically ascribing the deep soil temperature averaged over the surrounding lake shore land points as the lake surface temperature of the interior lake points. The averaging includes weighting with reciprocal distance between the designated lake point and the surrounding lake shore land points, to allow for an LST-gradient across the larger lakes. For the deep soil temperature the prognostic temperature of the third soil layer is adopted. This layer is supposed to represent air temperature fluctuations in the range of a week to a couple of weeks, which might be best connected to the response rate of a large water body. Obviously, this response time of LST is strongly determined by other characteristics of the lake like lake depth, internal lake circulation, the inflow of fresh, often cooler water from river tributaries, etc. None of these features is taken into consideration. In particular, a shallow lake like Lake IJssel might respond much faster to atmospheric conditions than the third soil layer does.

Once the LST is determined, a simple prescription is applied to diagnose lake ice fraction (LCI). It is essentially the same prescription that is used to allow for frozen soils. LCI at a lake grid point starts to build when the LST drops below 1°C , and reaches unity when LST becomes -2°C . Similarly a unity LCI starts to diminish when LST rises above -2°C and completely disappears when LST reaches 1°C . Hence, there is no hysteresis, nor are thermodynamic effects taken into account like the release of heat when lake ice is extending. Once lake ice is formed, a lake ice temperature profile is computed like for sea ice, with the same lake ice thickness assumed as for sea ice.

5. Dynamical Forcings

Numerical models for weather forecasting and climate prediction that are based on solving the primitive equations of the evolution of energy, mass and momentum all share essentially the same architecture. The resolved-scale model component, on the one hand, consists of calculating the effect of transport of the prognostic variables on a three-dimensional mesh of grid cells. This part of the model is referred to as the dynamics component or the adiabatic component, the former because this part of the model deals with the large-scale transport, the latter because the motions involved occur without generation or dissipation of heat. The subgrid-scale model component, on the other hand, accounts for the effect of unresolved processes on the evolution of resolved-scale prognostic variables. These accounts are called parameterizations since they are expressed in terms of the resolved-scale variables themselves. This part of the model is usually referred to as the physics component or the diabatic component, the latter because the processes involved induce exchange of heat with the environment. However, this is not entirely adequate, since e.g. sub-grid scale turbulent motions in the boundary layer are perfectly adiabatic as long as no phase changes are included. In probably all existing atmospheric models intended to represent processes on synoptic scales and mesoscales, parametric assumptions underlying the representation of subgrid-scale processes and their effect to the resolved scale are always introducing heterogeneity in horizontal dimensions (e.g. a grid cell is partly cloud filled, partly cloud free), whereas in the vertical direction atmospheric state variables are assumed homogeneous within a model layer. This likely explains why the outcome of numerical models can be much more sensitive to the vertical resolution than to the horizontal resolution, or put somewhat differently, introducing finer horizontal resolution results in similar solutions with finer detail primarily because of better resolved surface characteristics like topography and land sea mask. However, introducing finer vertical resolution may result in radically different solutions, in particular when it comes to representing thin cloud layers.

5.1 Single Column Models

From the above it may be understood that an atmospheric model can be considered as a horizontal grid of vertical columns. The vertical structure of each column is determined from the physics component of the model while communication between columns in the horizontal occurs through transport and numerical diffusion accounted for in the dynamics part of the model. It is also emphasized that the vertical columns do not mutually interact within the physics. From a slightly different perspective, each vertical column can be considered as an entity ruled by the package of physics parameterizations and somehow driven or controlled from the boundaries by external forcings. This notion introduced the concept of Single Column Model (SCM). At first, in the early nineties, the SCM was primarily seen as a useful tool for developing and testing parameterizations of physical processes. The great advantages of the SCM compared to a three-dimensional model are the much smaller demand - orders of magnitude smaller - of computational power and storing capacity, the reduction of complexity since the resolved-scale component of the model is ignored, and the much greater control that can be achieved in forcing the model to represent the processes of interest. SCMs did become particularly popular as a tool for comparison studies, and there exists a long list of papers reporting on SCM studies in which model results are compared either with observations or with finer-scale models like LES

or CRM, or just intercompared among SCMs. In general, the formulation of the external forcings in these type of studies is rather simple, i.e. a time-fixed profile of sources and sinks corresponding to lateral advection, large-scale subsidence and/or geostrophic wind speed. This information is somehow inferred from observations or a suitable model, and then greatly smoothed, to bring it into a simple shape. Most critical in this type of studies is that all SCMs apply the same forcing without reservation.

At KNMI, an effort is currently being made to establish a test bed of SCM versions carrying different parametric formulations that are processed in a semi-operational sense. The SCM runs are driven by the same external forcings on a daily basis and the output is evaluated with observations of a large number of parameters at Cabauw. In the long run, verification skill scores can be derived that provide an objective measure that allows deciding which SCM member in combination with the external forcings performs best at Cabauw. Hence, the external forcings to drive the SCM form a key component of the integration.

5.2 RACMO output for Single Column Models

To facilitate this type of SCM-integrations a three-day forecast with RACMO2.1 is performed twice a day and time series output that can serve as external forcing for the SCM is stored in a so-called dynamical forcings file (see Appendix A2) at designated grid points, e.g. the grid points nearest to Cabauw. The forecast run is initialized from an ECMWF analysis while ECMWF forecasts act as lateral boundary conditions. On initialization of the RACMO forecast run, information on prognostic surface/soil variables is directly inherited from a previous run without modification. The same applies to profiles of cloud parameters. The information that represents the external forcings required by the SCM is contained in the rate equations for the prognostic parameters. For any prognostic atmospheric parameter φ in model layer k the general expression for the local rate of change is:

$$\frac{\partial \varphi_k}{\partial t} = (D_\varphi)_k + (P_\varphi)_k + (K_\varphi)_k + (B_\varphi)_k,$$

where the tendency operators D , P , K , and B , represent the contributions from advective transport (or dynamics), physics, horizontal diffusion, and boundary relaxation, respectively. (Hereafter we assume that the designated grid point is in the interior of the model domain, where the effect of B is absent.) The right hand side reflects the computational ordering within one time step where the implicit horizontal diffusion operator K acts on the provisional model state that arises from applying $D+P$. The SCM is set up to mimic the evolution of a designated column from the 3-dimensional model by applying P , while D and K are supplied as external forcings. The variable φ stands for any of the multi-level prognostic variables, i.e. the horizontal wind vector \mathbf{v} , temperature T , specific humidity q_v , cloud liquid water q_l , cloud ice q_i , cloud fraction A , but also for the surface pressure p_s . Depending on φ , D takes different forms.

For any scalar quantity q , like e.g. specific humidity, but also cloud condensate, D becomes

$$D_q = -u \frac{\partial q}{\partial x} - v \frac{\partial q}{\partial y} - \dot{\eta} \frac{\partial q}{\partial \eta}$$

When applied to temperature, D becomes

$$D_T = -u \frac{\partial T}{\partial x} - v \frac{\partial T}{\partial y} - \dot{\eta} \frac{\partial T}{\partial \eta} + \frac{\kappa T_v}{1 + (\delta - 1)q_v} \left(\frac{\omega}{p} \right),$$

where $T_v = T(1 + (1/\varepsilon - 1)q_v)$ is the absolute virtual temperature, q_v the specific humidity (expressed in kg kg^{-1}), $\varepsilon = R_d/R_v \cong 0.61$ with R_d and R_v denoting the gas constants of dry air and water vapour, respectively, $\delta = c_{pv}/c_{pd} \cong 0.87$ with c_{pd} and c_{pv} denoting the specific heat constants of dry air and vapour at constant pressure, and $\kappa = R_d/c_{pd}$. The last term on the right hand side represents the effect of adiabatic compression or expansion of air to its temperature when being displaced vertically at a pressure vertical velocity ω (expressed in units Pa s^{-1}).

Depending on the SCM experiment one might be interested to apply, for example, only the horizontal part of the dynamic tendencies to the SCM and calculate the vertical advection from the vertical motion as given by the 3D-model combined with the vertical gradient as generated by the SCM model. To facilitate this option, parameters related to the vertical motion are also stored in the dynamical forcings file. In HIRLAM/RACMO, ω is computed from the hydrostatic equilibrium assumption and the continuity equation according to (Källén, 1996)

$$\omega = \frac{\partial p_s}{\partial t} + \int_{\eta}^1 \nabla_H \cdot (\mathbf{v} \frac{\partial p}{\partial \eta}) d\eta + \mathbf{v} \cdot \nabla p$$

In order to identify the contribution to the advection tendency associated to vertical motions we also need to know the hybrid vertical velocity $\dot{\eta}$ on half levels, which is usually obtained as

$$\dot{s} = \frac{1}{p_s} \left(\dot{\eta} \frac{\partial p}{\partial \eta} \right) = \left(1 - \frac{\partial p}{\partial p_s} \right) \frac{\partial \ln p_s}{\partial t} + \frac{1}{p_s} \int_{\eta}^1 \nabla_H \cdot (\mathbf{v} \frac{\partial p}{\partial \eta}) d\eta,$$

with $\dot{s} = 0$ at the vertical boundaries of the atmospheric column.

For the horizontal wind vector \mathbf{v} , D becomes

$$D_v = -\mathbf{v} \cdot \nabla_H \mathbf{v} - \dot{\eta} \frac{\partial \mathbf{v}}{\partial \eta} - f \mathbf{k} \times (\mathbf{v} - \mathbf{v}_g),$$

or expressed in wind components u and v ,

$$D_u = -u \frac{\partial u}{\partial x} - v \frac{\partial u}{\partial y} - \dot{\eta} \frac{\partial u}{\partial \eta} + f(v - v_g),$$

$$D_v = -u \frac{\partial v}{\partial x} - v \frac{\partial v}{\partial y} - \dot{\eta} \frac{\partial v}{\partial \eta} - f(u - u_g),$$

where f is the Coriolis parameter. \mathbf{v}_g denotes the geostrophic windvector, which is defined as (see Holton (1979,2004) for an elucidating introduction of the concept of geostrophic wind in the $\{x,y,p\}$ -coordinate frame)

$$\mathbf{v}_g = \mathbf{k} \times \frac{1}{\rho f} \nabla p,$$

or in terms of the geostrophic windcomponents u_g and v_g ,

$$u_g = \frac{1}{\rho f} \frac{\partial p}{\partial y},$$

$$v_g = -\frac{1}{\rho f} \frac{\partial p}{\partial x}.$$

An expression for \mathbf{v}_g in the $\{x,y,\eta\}$ -coordinate frame is obtained as follows:

$$\mathbf{v}_g = \mathbf{k} \times \frac{1}{f} \nabla_p \Phi,$$

where Φ is the geopotential obtained from the hydrostatic equation according to

$$d\Phi = -\rho dp = -R_d T_v d \ln p$$

and ∇_p is the horizontal gradient operator applied at constant pressure. The derivatives in the x -direction are related as

$$\left(\frac{\partial \Phi}{\partial x}\right)_\eta = \left(\frac{\partial \Phi}{\partial x}\right)_p + \left(\frac{\partial \Phi}{\partial p}\right)_x \left(\frac{\partial p}{\partial x}\right)_\eta$$

Substitution of the p -derivative of the hydrostatic relation at constant x yields

$$\left(\frac{\partial \Phi}{\partial x}\right)_p = \left(\frac{\partial \Phi}{\partial x}\right)_\eta + R_d T_v \left(\frac{\partial \ln p}{\partial x}\right)_\eta,$$

Hence, in the $\{x,y,\eta\}$ -coordinate frame the geostrophic wind vector is expressed as

$$\mathbf{v}_g = \mathbf{k} \times \frac{1}{f} (\nabla_\eta \Phi + R_d T_v \nabla_\eta \ln p).$$

Part of determining the advective tendency D_ϕ consists of application of a semi-implicit time scheme in solving the equations in order to suppress unwanted solutions (gravity waves, buoyancy waves). For this purpose a set of Helmholtz equations is solved. In the generation of advective tendency information the contributions from this procedure, referred to as the explicit/implicit adjustment, are stored separately in the dynamical forcings file. They are mostly (but not always) one order of magnitude smaller, and are only brought into account for the momentum components, temperature and surface pressure.

The horizontal diffusion operator K involves the solution of a 4th or 6th order implicit diffusion scheme which is carried out at the end of each timestep, after integration of the contributions from both the dynamics (adiabatic part) and the physics (diabatic part). K is applied to all parameters. As discussed by Lenderink et al. (2003), it was found beneficial for the representation of precipitation in the upstream region of mountain regions to reduce the diffusion coefficient of moisture by a factor of 10. Apart from this modification, the horizontal diffusion scheme has not been altered. The contributions from the horizontal diffusion tendencies are stored separately from the dynamical forcings, and it is left to the applicant of the SCM whether to include them in driving the single column model. In general, the K -terms are not that large compared to tendencies from advection or physics, but exceptions can arise near the surface, at land sea transitions, or in regions with large small-scale gradients e.g. due to strong but spatially and/or temporally intermittent convection. Under those conditions horizontal diffusion may generate large tendencies in order to smooth the spiky spatial structures.

5.3 Time-height structure of dynamical forcings

Figure 10 shows time-height diagrams for a number of fields and tendencies inferred from a 36-hr forecast run with RACMO at 18 km resolution. The shown parameters form a selection of parameters that has been used as guidelines in setting up the GABLS-3 case (GEWEX Atmospheric Boundary Layer Studies) designed for carrying out a detailed study of a stable boundary layer that was observed at Cabauw during the night of 1 to 2 July 2006. A discussion on the quality of model predicted tendencies corresponding to horizontal advection is given in Bosveld et al., 2008.

5.4 Numerical accuracy

Examination of time series information on dynamical forcings revealed very high noise levels at the time step scale for some of the parameters, in particular for the geostrophic wind speed components in the near-surface levels. This is illustrated in the bottom-right panel of Figure 11. In fact, noise levels are so large that an unfiltered time series of dynamical forcings is not suitable to act as driving information for an SCM run. Time-filtering the dynamical forcings at e.g. the hourly level or longer will certainly help in reducing the noise level. It should be realized, though, that time filtering will also smooth the dynamical forcings at time scales beyond the time step size and therefore alter the characteristics of the forcings.

Irrespective of the application, it is worthwhile finding out why several dynamical parameters are affected by such high noise levels, and whether this can be improved. A possible reason is the lack of accuracy of float operations. In the standard setup, float arithmetic in the dynamics component of the model - taken from HIRLAM - is carried out at single precision, whereas in the physics component - taken from ECMWF - it is carried out at double precision. Interface routines take care of consistent variable passing. In order to promote the float arithmetic in the dynamics component to double precision without altering the integer arithmetic a number of code changes had to be carried through in the HIRLAM code, the details of which are described in Appendix B

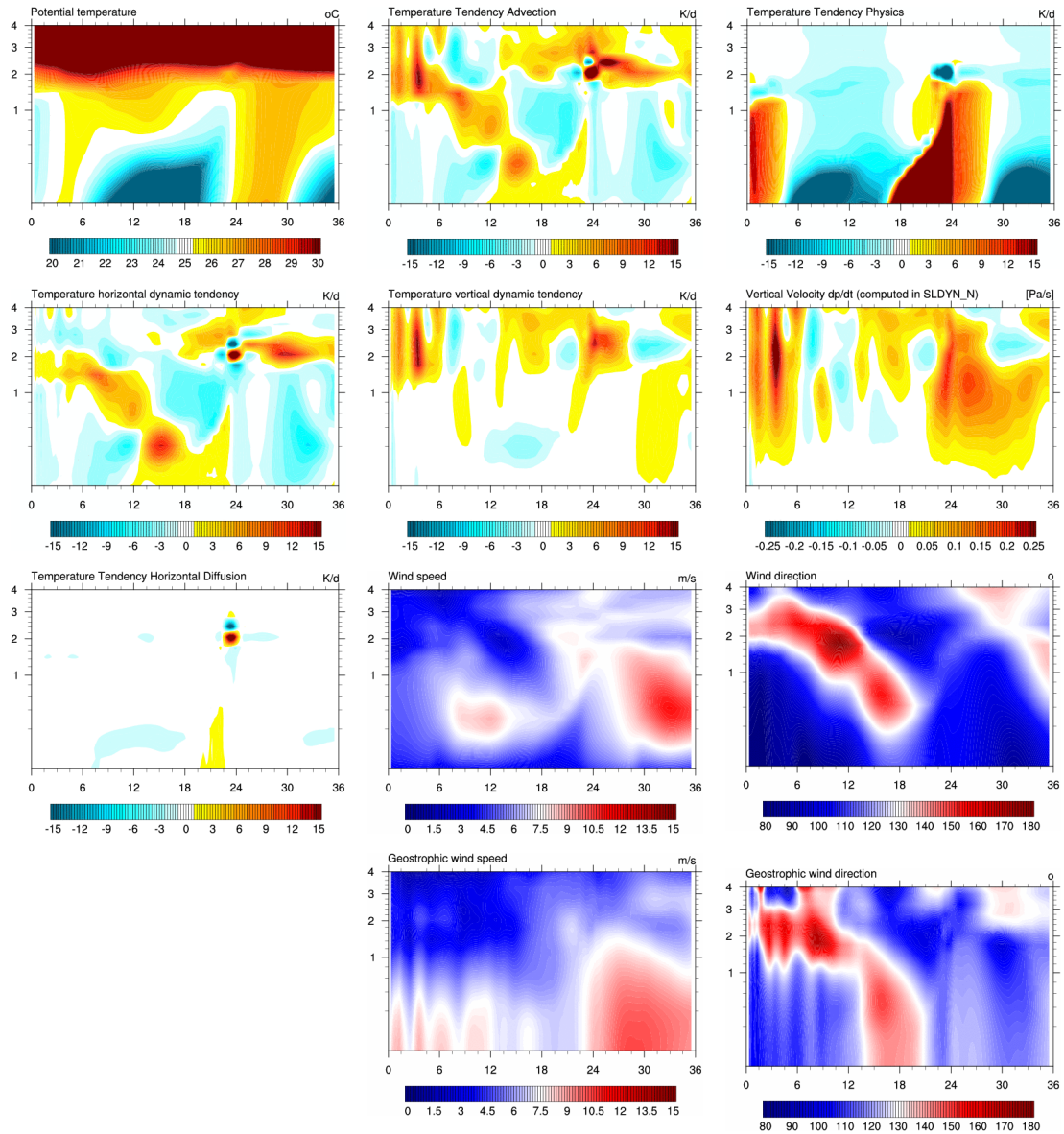


Figure 10: Time-height diagrams of various parameters derived at the Cabauw point from a 36-hr RACMO forecast run at 18km resolution initialized from an ECMWF-analysis verifying on 1 July 2007 12 UTC. Meaning and units of parameters is listed above the figure. The total temperature tendency advection (top-centre) is decomposed in a horizontal (2nd row left) and a vertical contribution (2nd row centre). The latter contains a vertical advection term and an expansion term which is controlled by the vertical velocity (2nd row right). Horizontal temperature diffusion (3rd row left) is very small apart from an exchange term at 2km after 24 hrs of integration due to the formation of an isolated cloud layer. The four figures in the 3rd and 4th row, centre and right illustrate the model wind speed and direction, and the geostrophic counterparts. All parameters are time filtered with a moving one-hour block function centered around the actual time.

After RACMO was made suitable for double precision float arithmetic, results obtained at both float precisions could be compared. Time series for a number of parameters are shown in Figure 11. As already mentioned above, the near-surface geostrophic wind component produced in single precision calculations exhibits very high noise levels – see curve labelled R4 UGEO40 (40 refers to model level 40 which is the lowest model level) in bottom right panel. In the time series produced by the double precision calculations – see curve labelled R8 UGEO40 in same panel – these large oscillations have completely vanished. The conclusion seems justified that the apparent high noise levels in some of the dynamical parameters are induced by lack of numerical accuracy in (some of) the float operations in the standard operational environment. While noise levels in the geostrophic wind components are very large at the lowest model level they reduce considerably at higher levels, e.g. at level 30 – about 1 km altitude – the amplitudes of the noise has decreased by a factor of 20. Noise is also found in the near-surface wind component itself, but in a modest amount (see Figure 11). The same applies to the vertical velocity but for this parameter the reduction in noise level with height is slower. Noise levels in the near-surface values of temperature and specific humidity are very small, and at higher levels not discernible. Likewise, surface pressure is also found entirely insensitive to the employed float

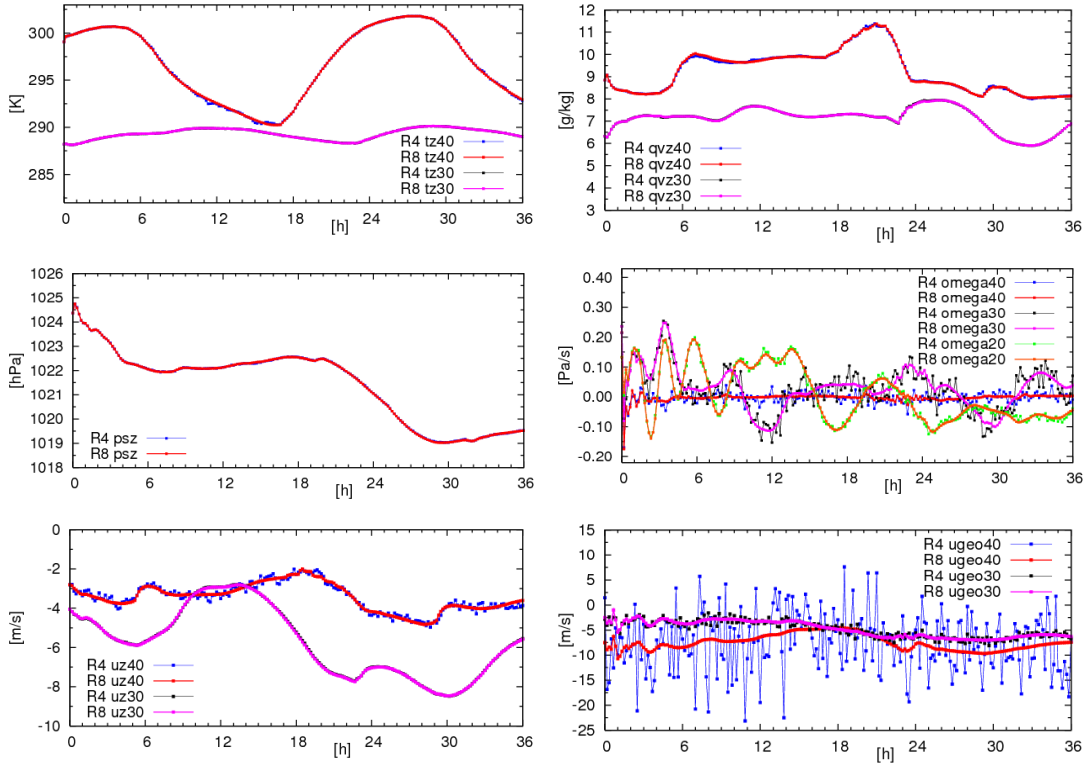


Figure 11: Time series obtained at single precision (R4) and double precision (R8) for the u -component of the geostrophic wind (UGEO), the wind component (UZ), the vertical velocity (OMEGA), the surface pressure (PSZ), the specific humidity (QVZ), and the temperature (T) at levels 40 (height $\sim 10\text{m}$), 30 (height $\sim 1\text{km}$) or 20 (height $\sim 5\text{km}$ – only vertical velocity). Time and location correspond to Figure 10.

precision. Hence, a reassuring conclusion seems justified that, in an overall sense, the model output obtained at double precision is not different from the result obtained with single precision arithmetic in the dynamics component.

6. Summary and Outlook

This report gives a status overview of the KNMI regional climate model RACMO version 2.1 with an emphasis on the elements that are new in this version. Version 2.1 has been built on its predecessor 2.0 (Lenderink et al., 2003) that was originally developed by merging the ECMWF physics package of cycle 23r4 into the dynamical kernel of HIRLAM 5.0.6. It is again pointed out that the report is not intended to provide a comprehensive technical description of the entire model, as such type of information can already be found in technical documentation elsewhere describing the originating HIRLAM (Undén et al., 2001) and ECMWF (White, 2004) components. However, modifications to the new version either relative to the originating sources or rather of a standalone nature are described in detail. In addition we have attempted to provide a comprehensive overview of the direct model output (DMO) produced by the model. This is done in the form of appendices.

RACMO2.1 has been the baseline version for the present-day and future climate integrations focussing on the European domain carried out within the frameworks of EU-ENSEMBLES and the initial phase of the national program Climate changes Spatial Planning. In addition, versions of RACMO2.1, supplied with parametric formulations specifically developed for the treatment of the ice cap surface have been extensively used in contemporary studies of Antarctica and Greenland (RAPID), or are going to be applied in studies on past and future climate of the Greenland ice cap (IPY).

While this report is written the development of a successor of RACMO2.1 is already entering its final stage. The dynamics component of the upcoming release, referred to as RACMO2.2, is kept unchanged. Parts of the physics, however, are drastically altered, as the baseline of the new version is formed by the ECMWF physics package from cycle 31r1. In particular, the deep convection parameterization has been considerably modified compared to previous cycles. Also the role of sub-grid scale orography on near-surface momentum dissipation has been considerably revised. A major change is the introduction of the externalized formulation of the surface/soil scheme, which involves significant changes on the level of code implementation. The new baseline of RACMO2.2 establishes a strong link with the ongoing developments of the global climate model EC-Earth, because this GCM also uses the forecast component of IFS-ECMWF cycle 31r1 as its atmospheric component.

Model developments initiated within the framework of CcSP will build on the baseline version of RACMO2.2. Amongst others these include the introduction of a turbulent kinetic energy (TKE) variable in the framework of the Eddy-Diffusivity Mass-Flux (EDMF) approach in representing boundary-layer processes, and the extension of the soil hydrology component of the surface/soil scheme HTESSEL with spatially heterogeneity of soil hydrology parameters, like root depth distribution, ground water table, etc.. Also the role of seasonal variations in leaf area index (LAI) to the surface energy balance is brought into account by allowing

spatial patterns of LAI to vary in time as inferred from satellite observations. To study the impact of the aerosol indirect effect on the model climate an initial step is set by implementing a cloud aerosol parameterisation that relates aerosol mass through cloud condensation nuclei number to the effective radius of cloud droplets (de Martino et al., 2008).

Issues that, based on experience with RACMO2.1, still need to be addressed include the introduction of a slab module that allows the sea surface temperatures of shallow coastal seas or lake surface temperatures to be interactively prognosed instead of being prescribed from a low-resolution global climate simulation. This is especially relevant for improving the consistency of high resolution climate integrations in coastal regions. Also, in the longer term it will certainly be considered to port updates or new components in the ECMWF physics new developments into RACMO. These include developments in the convective parameterizations, the new Short Wave radiative scheme based on RRTM (Rapid Radiative Transfer module), the McICA (Monte Carlo Independent Column Approximation) as a radically new approach to account for cloud overlap (both SW-RRTM and Mc-ICA are operational in the ECMWF model since Cy3 2r3), the incorporation of an urban tile, and the extension of the surface-soil scheme to interactively include components of the carbon cycle (CTESSEL).

Finally, in the more distant future, about three to five years from now, we expect that owing to the increase of computational power multi-annual climate-type integrations with RCMs will become feasible at horizontal resolutions at the 5 km scale. This will require certain adjustments to the model, e.g. the implementation of a non-hydrostatic kernel to account for resolved-scale transport because the approximation of hydrostatic equilibrium is no longer valid in this range of resolved scales. Also, part of the deep convection will be resolved at this resolution, which requires reformulation of the convective parametrisation scheme.

Appendix A: Model Output

Direct model output is stored in two forms:

1. 2-dimensional fields stored in ASIMOF-GRIB-formatted files each referring to a single instant in time. Temporal resolution typically varies between 1 to 24 hours. ASIMOF-GRIB is a special HIRLAM related version of the FM 92 GRIB (gridded binary) standard.
2. Time series of meteorological parameters at designated grid points stored in NetCDF (Network Common Data Format) formatted files.

Appendix A1: ASIMOF-GRIB formatted output

Table A1.1: List of 2-dimensional fields with instantaneous values stored in the model state file, also referred to as history file.

	Field	Units	Varname	par	lvt	lev
I/O	surface pressure	[Pa]	PS	1	105	0
I	surface geopotential	[m ² s ⁻²]	PHIS	6	105	0
I	sea surface temperature	[K]	SST	11	102	0
O	skin temperature tile j	[K]	TSKTI	11	1	itile
I/O	skin temperature	[K]	TL	11	105	0
O	2 meter temperature	[K]	TCFL	11	105	2
I/O	soil temperature layer k	[K]	TSA	11	105	1000-k
I/O	multi-layer temperature	[K]	T	11	109	ilev
O	2 meter dewpoint	[K]	DCFL	17	105	2
I/O	sea ice temperature layer k	[K]	TIA	21	105	1000-k
O	10 meter zonal wind speed	[m s ⁻¹]	UCFL	33	105	10
I/O	multi-layer zonal wind speed	[m s ⁻¹]	U	33	109	ilev
O	10 meter meridional wind speed	[m s ⁻¹]	VCFL	34	105	10
I/O	multi-layer meridional wind speed	[m s ⁻¹]	V	34	109	ilev
(O)	vertical velocity	[Pa s ⁻¹]	VERVEL	39	109	ilev
O	2 meter specific humidity	[kg kg ⁻¹]	QCFL	51	105	2
I/O	specific humidity	[kg kg ⁻¹]	Q	51	109	ilev
O	2 meter relative humidity	[0..1]	RHCFL	52	105	0
O	total precipitation flux	[kg m ⁻² s ⁻¹]	SRTDG(.,1+2)	61	105	0
O	large-scale precipitative flux	[kg m ⁻² s ⁻¹]	SRTDG(.,2)	62	105	0
O	area fraction LS precipitation	[0..1]	RILSPF	62	105	1
O	convective precipitative flux	[kg m ⁻² s ⁻¹]	SRTDG(..1)	63	105	0
I/O	snow pack depth	[m w.eq.]	SNS	66	105	0
O	snow cover fraction (sea ice excl.)	[0..1]	FRTI(.,5+7)	66	105	1
O	total cloud cover	[0..1]	TCC	71	105	0
O	high-level cloud cover	[0..1]	HCC	71	105	1
O	medium-level cloud cover	[0..1]	MCC	71	105	2
O	low-level cloud cover	[0..1]	LCC	71	105	3
O	convective cloud cover	[0..1]	CCC	71	105	4
I/O	specific cloud fraction	[0..1]	CVAR(.,3)	71	109	ilev
O	cloud liquid water path	[kg m ⁻²]	QLI	76	105	0

Table A1.1 (Continued): List of 2-dimensional fields with instantaneous values stored in the model state file, also referred to as history file.

	Field	Units	Varname	par	lvt	lev
I/O	specific liquid water	[kg kg ⁻¹]	CVAR(.,1)	76	109	ilev
O	cloud ice water path	[kg m ⁻²]	QII	77	105	o
I/O	specific ice	[kg kg ⁻¹]	CVAR(.,2)	77	109	ilev
O	relative areal fraction tile j	[o..1]	FRTI	81	1	itile
I	land sea mask	[o..1]	LSM	81	105	o
I/O	roughness length of heat (LOG)	[m]	AZoH (LZoH)	82	105	o
I/O	roughness length of momentum	[m]	AZoM	83	105	o
I	background surface albedo	[o..1]	ALBF	84	105	o
O	surface albedo	[o..1]	ALB	84	105	o
I/O	soil water content layer k	[m ³ m ⁻³]	WSA	86	105	1000-k
(I)	fraction of urbanisation	[o..1]	-	89	105	o
O	fraction of sea ice	[o..1]	CI	91	102	o
I/O	fraction of lakes	[o..1]	FRLAKE	92	105	o
O	convective mass flux updrafts	[kg m ⁻² s ⁻¹]	SRTDG(.,17)	116	109	ilev
O	convective mass flux downdrafts	[kg m ⁻² s ⁻¹]	SRTDG(.,18)	117	109	ilev
O	surface latent heat flux	[Wm ⁻²]	AHFL	121	105	o
O	surface sensible heat flux tile j	[Wm ⁻²]	AHFSTI	122	1	itile
O	surface sensible heat flux	[Wm ⁻²]	AHFS	122	105	o
O	surface momentum flux	[kg m ⁻¹ s ⁻²]	MOMF	128	105	o
I/O	snow albedo	[o..1]	ASN	156	105	o
I/O	snow density	[kg m ⁻³]	RSN	157	105	o
O	friction velocity	[m]	USTAR	159	105	o
O	heat flux soil layer 1 → 2	[Wm ⁻²]	SRTDG(.,25)	162	105	o
O	10 meter windspeed	[m s ⁻¹]	-	171	105	10
O	net surface SW radiation	[Wm ⁻²]	SRTDG(.,11)	176	105	o
O	incoming surface SW radiation	[Wm ⁻²]	SRTDG(.,13)	176	105	1
O	net surface LW radiation	[Wm ⁻²]	SRTDG(.,10)	177	105	o
O	downwelling surface LW radiation	[Wm ⁻²]	SRTDG(.,12)	177	105	1
O	net top-of-atmosphere SW radiation	[Wm ⁻²]	SRTDG(.,15)	178	105	o
O	incoming top-of-atmosphere SW radiation	[Wm ⁻²]	SRTDG(.,16)	178	105	1
O	net top-of-atmosphere LW radiation	[Wm ⁻²]	SRTDG(.,14)	179	105	o
O	surface U-momentum stress tile j	[kg m ⁻¹ s ⁻²]	USTRTI	180	1	itile
O	surface U-momentum flux	[kg m ⁻¹ s ⁻²]	SRTDG(.,7)	180	105	o
O	surface V-momentum stress tile j	[kg m ⁻¹ s ⁻²]	VSTRTI	181	1	itile
O	surface V-momentum flux	[kg m ⁻¹ s ⁻²]	SRTDG(.,8)	181	105	o
O	surface evaporation tile j	[kg m ⁻² s ⁻¹]	EVAPTI	182	1	itile
I	coverage of high vegetation	[o..1]	CVH	188	105	1
I	coverage of low vegetation	[o..1]	CVL	188	105	2
I	standard deviation of height	[m] ^{*)}	HSTD	189	105	o
I	orographic anisotropy	[o..1]	HGAMMA	189	105	1
I	orographic orientation	[radians]	HTHETA	189	105	2
I	orographic mean slope	[o..1]	HSIG	189	105	3

Table A1.1 (Continued): List of 2-dimensional fields with instantaneous values stored in the model state file, also referred to as history file.

	Field	Units	Varname	par	lvt	lev
I/O	skin reservoir content	[m w.eq.]	WL	194	105	0
O	outgoing top-of-atmosphere SW radiation	[Wm ⁻²]	SRTDG(.,15-16)	203	105	0
O	reflected surface SW radiation	[Wm ⁻²]	SRTDG(.,11-13)	204	105	0
O	emitted surface LW radiation	[Wm ⁻²]	SRTDG(.,10-12)	205	105	0
I/O	snow pack temperature	[K]	TSN	206	105	0
O	net "clear sky" top-of-atmosphere SW radiation	[Wm ⁻²]	SRTDG(.,21)	207	105	0
O	net "clear sky" top-of-atmosphere LW radiation	[Wm ⁻²]	SRTDG(.,23)	208	105	0
O	net "clear sky" surface SW radiation	[Wm ⁻²]	SRTDG(.,22)	209	105	0
O	net "clear sky" surface LW radiation	[Wm ⁻²]	SRTDG(.,24)	210	105	0
I	forest coverage (not used)	[-]	FRF	212	105	0
I	type of high vegetation	[-]	TVH	212	105	1
I	type of low vegetation	[-]	TVL	212	105	2
O	10 meter wind gust	[m s ⁻¹]	WI10FG	213	105	10
O	convective cloud top	[mod level]	HCTOP	217	105	0
O	convective cloud base	[mod level]	HCBAS	217	105	1
O	boundary layer height	[m]	PBLH	224	105	0
O	vertically integrated water vapour	[kg m ⁻²]	QVI	230	105	0
O	vertically integrated cloud content	[kg m ⁻²]	QCI	231	105	0

*) in former releases, field 189-105-0 contains the orographic variance in m²

Table A1.2: list of 2-dimensional fields with accumulated and extreme values stored in the md-file.

	Field	Units	par	lvt	lev
O	total precipitation	[kg m ⁻²]	61	105	0
O	large-scale precipitation	[kg m ⁻²]	62	105	0
O	convective precipitation	[kg m ⁻²]	63	105	0
O	precipitation duration	[s]	69	105	0
O	cloud liquid water path	[kg m ⁻² s]	76	105	0
O	cloud ice path	[kg m ⁻² s]	77	105	0
O	potential vorticity on isentropic planes (default at 315, 330, 350, 380, 405 K)	PV-units = 1.e-6 *[K m ² kg ⁻¹ s ⁻¹]	120	4	
O	surface latent heat flux	[Wm ⁻² s]	121	105	0
O	surface latent heat flux snow-free	[Wm ⁻² s]	121	105	1
O	surface latent heat flux snow-cover	[Wm ⁻² s]	121	105	2
O	surface sensible heat flux	[Wm ⁻² s]	122	105	0
O	total snow fall	[kg m ⁻²]	144	105	0
O	convective snow fall	[kg m ⁻²]	144	105	1

Table A1.2 (Continued): list of 2-dimensional fields with accumulated and extreme values stored in the md-file.

Field	Units	par	lvt	lev
O large-scale snow fall	[kg m ⁻²]	144	105	2
O turbulent dissipation	[Wm ⁻² s]	145	105	0
O total runoff	[kg m ⁻²]	160	105	0
O runoff from top soil layer	[kg m ⁻²]	160	105	1
O runoff from deeper layers [2-4]	[kg m ⁻²]	160	105	2
O water flux soil layer 1 → 2	[kg m ⁻²]	161	105	0
O heat flux soil layer 1 → 2	[Wm ⁻² s]	162	105	0
O sunshine duration	[s]	175	105	0
O net surface SW radiation	[Wm ⁻² s]	176	105	0
O incoming surface SW radiation	[Wm ⁻² s]	176	105	1
O net surface LW radiation	[Wm ⁻² s]	177	105	0
O downwelling surface LW radiation	[Wm ⁻² s]	177	105	1
O net top-of-atmosphere SW radiation	[Wm ⁻² s]	178	105	0
O incoming top-of-atmosphere SW radiation	[Wm ⁻² s]	178	105	1
O net top-of-atmosphere LW radiation	[Wm ⁻² s]	179	105	0
O surface U-momentum flux	[kg m ⁻¹ s ⁻¹]	180	105	0
O surface V-momentum flux	[kg m ⁻¹ s ⁻¹]	181	105	0
O surface evaporation	[kg m ⁻²]	182	105	0
O surface evaporation liquid	[kg m ⁻²]	182	105	1
O surface evaporation solid	[kg m ⁻²]	182	105	2
O gravity wave drag U-stress	[kg m ⁻¹ s ⁻¹]	195	105	0
O gravity wave drag V-stress	[kg m ⁻¹ s ⁻¹]	196	105	0
O gravity wave drag dissipation	[Wm ⁻² s]	197	105	0
O maximum 2 meter temperature	[K]	201	105	2
O minimum 2 meter temperature	[K]	202	105	2
O outgoing top-of-atmosphere surface SW radiation	[Wm ⁻² s]	203	105	0
O reflected surface SW radiation	[Wm ⁻² s]	204	105	0
O emitted surface LW radiation	[Wm ⁻² s]	205	105	0
O net “clear sky” top-of-atmosphere SW radiation	[Wm ⁻²]	207	105	0
O net “clear sky” top-of-atmosphere LW radiation	[Wm ⁻²]	208	105	0
O net “clear sky” surface SW radiation	[Wm ⁻²]	209	105	0
O net “clear sky” surface LW radiation	[Wm ⁻²]	210	105	0
O maximum 10 meter wind gust	[m s ⁻¹]	213	105	0
O maximum surface temperature	[K]	214	105	0
O minimum surface temperature	[K]	215	105	0
O maximum 10 meter wind speed	[m s ⁻¹]	216	105	10
O water flux corresponding to snow melt	[kg m ⁻²]	218	105	0
O maximum 2 meter relative humidity	[0..1]	228	105	2
O minimum 2 meter relative humidity	[0..1]	229	105	2
O water vapour column	[kg m ⁻² s]	230	105	0
O convergence of water vapour column	[kg m ⁻² s ⁻¹ s]	230	105	1
O change in water vapour column due to advection	[kg m ⁻² s ⁻¹ s]	230	105	2
O change in water vapour column due to physics	[kg m ⁻² s ⁻¹ s]	230	105	3

Table A1.2 (Continued): list of 2-dimensional fields with accumulated and extreme values stored in the md-file.

	Field	Units	par	lvt	lev
O	change in water vapour column due to horizontal diffusion	[kg m ⁻² s ⁻¹ s]	230	105	4
O	change in water vapour column due to boundary relaxation	[kg m ⁻² s ⁻¹ s]	230	105	5
O	convergence of liquid water + ice path	[kg m ⁻² s ⁻¹ s]	231	105	1
O	change in liquid water + ice path due to advection	[kg m ⁻² s ⁻¹ s]	231	105	2
O	change in liquid water + ice path due to physics	[kg m ⁻² s ⁻¹ s]	231	105	3
O	change in liquid water + ice path due to horizontal diffusion	[kg m ⁻² s ⁻¹ s]	231	105	4
O	change in liquid water + ice path due to making LWC&IWC positive	[kg m ⁻² s ⁻¹ s]	231	105	6
O	zonal flux of water vapour column	[kg m ⁻¹ s ⁻¹ s]	233	105	0
O	meridional flux of water vapour column	[kg m ⁻¹ s ⁻¹ s]	234	105	0

Table A1.3: list of 2-dimensional fields with accumulated flux profiles stored in the px-file

	Field	Units	Varname	par	lvt	lev
I	surface geopotential	[m ² s ⁻²]	PHIS	6	105	0
O	large-scale rain flux	[kg m ⁻²]		62	109	k=1..nlev+1
O	convective rain flux	[kg m ⁻²]		63	109	k=1..nlev+1
O	convective mass flux updrafts	[kg m ⁻²]		116	109	k=1..nlev+1
O	convective mass flux downdrafts	[kg m ⁻²]		117	109	k=1..nlev+1
O	convective flux of specific humidity	[kg m ⁻²]		118	109	k=1..nlev+1
O	convective flux of dry static energy	[Wm ⁻² s]		119	109	k=1..nlev+1
O	turbulent flux of dry static energy	[Wm ⁻² s]		122	109	k=1..nlev+1
O	convective condensation flux ice	[kg m ⁻²]		123	109	k=1..nlev+1
O	convective condensation flux liquid water	[kg m ⁻²]		124	109	k=1..nlev+1
O	stratiform condensation flux ice	[kg m ⁻²]		125	109	k=1..nlev+1
O	stratiform condensation flux liquid water	[kg m ⁻²]		125	109	k=1..nlev+1
O	convective snow flux	[kg m ⁻²]		143	109	k=1..nlev+1
O	large-scale snow flux	[kg m ⁻²]		144	109	k=1..nlev+1
O	measure of surface pressure Δp_s ' ^{*)}	[Pa s]		152	105	0
O	net SW radiative flux	[Wm ⁻² s]		176	109	k=1..nlev+1
O	net LW radiative flux	[Wm ⁻² s]		177	109	k=1..nlev+1
O	turbulent flux of U-momentum	[kg m ⁻¹ s ⁻¹]		180	109	k=1..nlev+1
O	turbulent flux of V-momentum	[kg m ⁻¹ s ⁻¹]		181	109	k=1..nlev+1
O	turbulent flux of specific humidity	[kg m ⁻²]		182	109	k=1..nlev+1
O	gravity wave drag flux of U-momentum	[kg m ⁻¹ s ⁻¹]		195	109	k=1..nlev+1

Table A1.3 (Continued): list of 2-dimensional fields with accumulated flux profiles stored in the px-file

	Field	Units	Varname	par	lvt	lev
O	gravity wave drag flux of V-momentum	[kg m ⁻¹ s ⁻¹]		196	109	k=1..nlev+1
O	convective flux of U-momentum	[kg m ⁻¹ s ⁻¹]		198	109	k=1..nlev+1
O	convective flux of V-momentum	[kg m ⁻¹ s ⁻¹]		199	109	k=1..nlev+1

^{*)} measure of surface pressure is taken as $\Delta p_s' = p_s \exp(\text{PHIS}/(R_d T_o)) - p_o$, with PHIS the surface geopotential in m² s⁻², $R_d = 287.04 \text{ JK}^{-1} \text{ kg}^{-1}$, $p_o = 101325 \text{ Pa}$, and $T_o = 273.16 \text{ K}$.

Table A1.4: list of 2-dimensional fields with accumulated tendency profiles stored in the td-file.

	Field	Units	par	lvt	lev
O	surface pressure (accumulated)	[Pa s]	1	105	0
O	surface pressure tendency advection	[Pa s ⁻¹ s]	1	105	1
O	surface pressure tendency physics	[Pa s ⁻¹ s]	1	105	2
O	surf .pres. tend. horizontal diffusion	[Pa s ⁻¹ s]	1	105	3
O	surf .pres. tend. expl/impl adjustment	[Pa s ⁻¹ s]	1	105	4
O	surf .pres. tend. boundary relaxation	[Pa s ⁻¹ s]	1	105	5
O	temperature (accumulated)	[K s]	210	109	k=1..nlev
O	temperature tendency advection	[K s ⁻¹ s]	211	109	k=1..nlev
O	temperature tendency physics	[K s ⁻¹ s]	212	109	k=1..nlev
O	temperature tend. horizontal diffusion	[K s ⁻¹ s]	213	109	k=1..nlev
O	temperature tend. expl/impl adjustment	[K s ⁻¹ s]	214	109	k=1..nlev
O	temperature tend. boundary relaxation	[K s ⁻¹ s]	215	109	k=1..nlev
O	specific humidity (accumulated)	[kg kg ⁻¹ s]	220	109	k=1..nlev
O	specific humidity tendency advection	[kg kg ⁻¹ s ⁻¹ s]	221	109	k=1..nlev
O	specific humidity tendency physics	[kg kg ⁻¹ s ⁻¹ s]	222	109	k=1..nlev
O	spec. hum. tend. horizontal diffusion	[kg kg ⁻¹ s ⁻¹ s]	223	109	k=1..nlev
O	spec. hum. tend. boundary relaxation	[kg kg ⁻¹ s ⁻¹ s]	225	109	k=1..nlev
O	cloud liquid water (accumulated)	[kg kg ⁻¹ s]	230	109	k=1..nlev
O	cloud liquid water tendency advection	[kg kg ⁻¹ s ⁻¹ s]	231	109	k=1..nlev
O	cloud liquid water tendency physics	[kg kg ⁻¹ s ⁻¹ s]	232	109	k=1..nlev
O	cloud liquid water horizontal diffusion	[kg kg ⁻¹ s ⁻¹ s]	233	109	k=1..nlev
O	cloud ice (accumulated)	[kg kg ⁻¹ s]	240	109	k=1..nlev
O	cloud ice tendency advection	[kg kg ⁻¹ s ⁻¹ s]	241	109	k=1..nlev
O	cloud ice tendency physics	[kg kg ⁻¹ s ⁻¹ s]	242	109	k=1..nlev
O	cloud ice horizontal diffusion	[kg kg ⁻¹ s ⁻¹ s]	243	109	k=1..nlev
O	cloud fraction (accumulated)	[s]	250	109	k=1..nlev
O	cloud fraction tendency advection	[s ⁻¹ s]	251	109	k=1..nlev
O	cloud fraction tendency physics	[s ⁻¹ s]	252	109	k=1..nlev
O	cloud fraction horizontal diffusion	[s ⁻¹ s]	253	109	k=1..nlev

Table A1.5: list of 2-dimensional fields intended for operational verification stored in the ve-file

	Field	Units	par	lvt	lev
O	mean sea level pressure	[Pa]	1	103	0
O	surface pressure	[Pa]	1	105	0
O	geopotential	[m ² s ⁻²]	6	100	plev ^{*)}
O	temperature	[K]	11	100	plev ^{*)}
O	2 meter temperature	[K]	11	105	2
O	dew point temperature	[K]	17	100	plev ^{*)}
O	2 meter dewpoint	[K]	17	105	2
O	zonal wind speed	[m s ⁻¹]	33	100	plev ^{*)}
O	10 meter zonal wind speed	[m s ⁻¹]	33	105	10
O	meridional wind speed	[m s ⁻¹]	34	100	plev ^{*)}
O	10 meter meridional wind speed	[m s ⁻¹]	34	105	10
O	vertical velocity	[Pa s ⁻¹]	39	109	plev ^{*)}
O	specific humidity	[kg kg ⁻¹]	51	109	plev ^{*)}
O	relative humidity	[%]	52	100	plev ^{*)}
O	total precipitation	[kg m ⁻²]	61	105	0
O	cloud fraction	[0..1]	71	100	plev ^{*)}
O	total cloud cover	[0..1]	71	105	0
O	cloud liquid water	[kg kg ⁻¹]	76	100	plev ^{*)}
O	cloud ice	[kg kg ⁻¹]	77	100	plev ^{*)}
O	cloud liquid water + ice	[kg kg ⁻¹]	231	100	plev ^{*)}

^{*)} plev designates pressure level; standard selection is 100,300,500,700,850,925,1000 hPa

Appendix A2: NetCDF formatted output

Time series of meteorological parameters at designated grid points are directly exported from the model into NetCDF formatted files. The information is stored into two files, one containing single-level fields, the other multi-level fields. The temporal resolution of this output is set by the user. Standard output – model state variables and model fluxes - include all fields listed in tables A1.1, A1.2, A1.3, and A1.5.

An additional stream of time series output collects information that is needed to drive an integration with a local atmospheric model at a designated location (see Section 5). This time series file, referred to as the dynamical forcings file, is also NetCDF formatted. Information is stored every model time step. The file content is described in Table A2.1.

Table A2.1: List of parameters contained in dynamical forcings file (NetCDF format)

	Parameter	Units	NetCDF name	Dimension
I	geographic longitude receptor point	deg_E	lon	point
I	geographic latitude receptor point	deg_N	lat	point
O	angle between geographic grid and rotated lat-lon model grid	degrees	dir	point

Table A2.1 (Continued): List of parameters contained in dynamical forcings file (NetCDF format)

Parameter	Units	NetCDF name	Dimension
I grid index	-	pos	point
I receptor point name (if provided)	-	site	point:strlen
I full level hybrid pressure parameter	Pa	afull	levf
I full level hybrid sigma parameter	-	bfull	levf
I half level hybrid pressure parameter	Pa	ahalf	levh
I half level hybrid sigma parameter	-	bhalf	levh
O elapsed time since reference	[s]	time	time [†]
O date of verifying time	[yyymmdd]	date	time
O hour-minute-second of verifying time	[hhmmss]	hms	time
I surface geopotential	[m ² s ⁻²]	phis	point
I land sea mask	[-]	lsm	point
O surface pressure	[Pa]	psz	point:time
O surface pressure tendency advection	[Pa s ⁻¹]	dpsdt_dyn	point:time
O surface pressure tendency physics	[Pa s ⁻¹]	dpsdt_phys	point:time
O surf .pres. tend. horizontal diffusion	[Pa s ⁻¹]	dpsdt_hdf	point:time
O surf .pres. tend. expl/impl adjustment	[Pa s ⁻¹]	dpsdt_adj	point:time
O surf .pres. tend. boundary relaxation	[Pa s ⁻¹]	dpsdt_bnd	point:time
O zonal wind speed	[m s ⁻¹]	uz	point:levf:time
O zonal wind speed tendency advection	[m s ⁻¹ s ⁻¹]	dudt_dyn	point:levf:time
O zonal wind speed tendency physics	[m s ⁻¹ s ⁻¹]	dudt_phys	point:levf:time
O zonal wind speed tendency horizontal advection	[m s ⁻¹ s ⁻¹]	dudt_hdf	point:levf:time
O zonal wind speed tendency expl/impl adjustment	[m s ⁻¹ s ⁻¹]	dudt_adj	point:levf:time
O zonal wind speed tendency boundary relaxation	[m s ⁻¹ s ⁻¹]	dudt_bnd	point:levf:time
O meridional wind speed	[m s ⁻¹]	vz	point:levf:time
O meridional wind speed tendency advection	[m s ⁻¹ s ⁻¹]	dvdt_dyn	point:levf:time
O meridional wind speed tendency physics	[m s ⁻¹ s ⁻¹]	dvdt_phys	point:levf:time
O meridional wind speed tendency horizontal advection	[m s ⁻¹ s ⁻¹]	dvdt_hdf	point:levf:time
O meridional wind speed tendency expl/impl adjustment	[m s ⁻¹ s ⁻¹]	dvdt_adj	point:levf:time
O meridional wind speed tendency boundary relaxation	[m s ⁻¹ s ⁻¹]	dvdt_bnd	point:levf:time
O temperature	[K]	tz	point:levf:time
O temperature tendency advection	[K s ⁻¹]	dttd_dyn	point:levf:time
O temperature tendency physics	[K s ⁻¹]	dttd_phys	point:levf:time
O temperature tend. horizontal diffusion	[K s ⁻¹]	dttd_hdf	point:levf:time
O temperature tend. expl/impl adjustment	[K s ⁻¹]	dttd_adj	point:levf:time
O temperature tend. boundary relaxation	[K s ⁻¹ s]	dttd_bnd	point:levf:time
O specific humidity	[kg kg ⁻¹]	qvz	point:levf:time
O specific humidity tendency advection	[kg kg ⁻¹ s ⁻¹]	dqvdt_dyn	point:levf:time
O specific humidity tendency physics	[kg kg ⁻¹ s ⁻¹]	dqvdt_phys	point:levf:time
O spec. hum. tend. horizontal diffusion	[kg kg ⁻¹ s ⁻¹]	dqvdt_hdf	point:levf:time
O spec. hum. tend. boundary relaxation	[kg kg ⁻¹ s ⁻¹]	dqvdt_bnd	point:levf:time

Table A2.1 (Continued): List of parameters contained in dynamical forcings file (NetCDF format)

Parameter	Units	NetCDF name	Dimension
O cloud liquid water	[kg kg ⁻¹]	qlz	point:levf:time
O cloud liquid water tendency advection	[kg kg ⁻¹ s ⁻¹]	dqldt_dyn	point:levf:time
O cloud liquid water tendency physics	[kg kg ⁻¹ s ⁻¹]	dqldt_phys	point:levf:time
O cloud liquid water horizontal diffusion	[kg kg ⁻¹ s ⁻¹]	dqldt_hdf	point:levf:time
O cloud ice (accumulated)	[kg kg ⁻¹ s]	qiz	point:levf:time
O cloud ice tendency advection	[kg kg ⁻¹ s ⁻¹]	dqidt_dyn	point:levf:time
O cloud ice tendency physics	[kg kg ⁻¹ s ⁻¹]	dqidt_phys	point:levf:time
O cloud ice horizontal diffusion	[kg kg ⁻¹ s ⁻¹]	dqidt_hdf	point:levf:time
O cloud fraction (accumulated)	[]	clz	point:levf:time
O cloud fraction tendency advection	[s ⁻¹]	dcldt_dyn	point:levf:time
O cloud fraction tendency physics	[s ⁻¹]	dcldt_phys	point:levf:time
O cloud fraction horizontal diffusion	[s ⁻¹]	dcldt_hdf	point:levf:time
O full level geometric height	[m]	height	point:levf:time
O pressure vertical velocity	[Pa s ⁻¹]	omega ^{*)}	point:levf:time
O etadot dp/deta ₁ /psurf	[s ⁻¹]	sdot ^{*)}	point:levh:time
O zonal geostrophic wind speed	[m s ⁻¹]	ugeo ^{*)}	point:levf:time
O meridional geostrophic wind speed	[m s ⁻¹]	vgeo ^{*)}	point:levf:time

^{†)} instead of “time” the temporal dimension is denoted “tim” in previous versions

^{*)} the parameter omega is calculated in routine SLDYN.f, the result of an alternative computation, denoted as omega2, is calculated in routine OMCOMP.f

^{*)} the parameter sdot, determined on half levels, is computed in COMPED.f

^{*)} the parameters ugeo and vgeo are computed in routine SLDYN.f, the result of an alternative computation, denoted as ugeo2 and vgeo2, is calculated in routine UVGEO.f

Appendix A3: ASIMOF-GRIB to NetCDF converter

In contribution to the ENSEMBLES project a Fortran90-based post-processing tool `asim2cdf` has been developed for the conversion of ASIMOF-GRIB-formatted model output into the NetCDF formatted output, which is a more convenient format for end users outside the HIRLAM/RACMO community. An additional and very important advantage of the conversion is that the content per file is reorganized from a multi-parameter content per (instant of) time in the ASIMOF files into a multi-time level content per parameter in the NetCDF files. The spatial structure remains the same. The post processing conversion tool is capable of performing a number of simple arithmetic operations. Given the temporal frequency of the data in the NetCDF formatted output (e.g. one month, one day, one hour) the conversion tool is able to compute the mean value of a quantity averaged or accumulated over the time interval, determine the minimum or maximum value, or simply return an instantaneous value. It can operate on scalars, but also on (staggered) components of a vector, thereby transforming the components or the direction of the vector from a rotated latitude-longitude grid, commonly used in RCMs, to a regular geographic grid. The post-processing tool can also operate on a pre-selected rectangular subdomain of the full domain. Usually, the conversion tool acts on a month of output data, but it can also act on shorter or longer intervals. The tool sequentially processes a list of parameters, each of them contained in one of the tables of Appendix A1. As its structure is

now, the tool can not combine parameters into a new parameter. For such purpose, additional, much more specific post-processing software, coded in either NCL or Fortran, is available or needs to be developed.

Appendix B: Double precision float arithmetic

In the standard installation, the dynamics component of the model, which is taken from HIRLAM, performs float operations at single precision (REAL*4), while the physics component, taken from ECMWF, performs float operations at double precision (REAL*8). This distinction is taken care of in the interface routines `pre_callpar.F90`, `setup_ph.ecmwf.F90` and `updtim_red.F90`. In these routines double sets of reals are declared, one set for each precision type, and assigned values are copied back and forth. Concerning integers, both model components perform INTEGER*4 arithmetic.

The default architecture of the HIRLAM model system does not allow real and integer variables to have different word length, hence promoting the real variables from single to double precision requires the Fortran compiler to have the capacity of performing INTEGER*8 arithmetic. This option is not always available, dependent on platform or compiler. To avoid this potential obstacle and yet be able to carry out float computations in the dynamics component at double precision we have disentangled the float and integer operations in the model part taken from HIRLAM wherever this was causing problems. It requires the following adjustments in the model and in the compiler environment.

Model:

1. Argument passed to routine `SECOND.f` must be a REAL*4. This affects routines `HLPROG.f`, `GEMINI_N.f`, `RESTART_N.f` and `TIMER.f` in library *grdy*.
2. The declarations of real and integer components of the DDR-record must be disentangled. This is done in the common-block definition `COMDDR.inc` (libraries *grw1* and *gdry*) by introducing the record sizes `mddrszR` and `mddrszI` with appropriate lengths:


```
PARAMETER(mddrszI=3*jpnslfx+2*jpnmlfx+1*jplevx+50)
PARAMETER(mddrszR=6*jpnslfx+3*jpnmlfx+4*jplevx+40+550)
```

Related modifications must be carried through in the following library routines:

```
grdy: GROPLOC.f
grw1: AS2DDR.f, PRIDDR.f
prpo: POSTPP_N.f, PUTGRB_PHEC.f, SETDDR.f, DESTAG.f,
      UVSTAG.f
```

3. Statements equivalencing reals and integers must be removed, while subsequent declarations of, and assignments to reals and/or integers must be made explicit. This affects quite a few lines, in particular where missing data indicators are defined. Also, it affects a number of arguments in calling entry routines in library *gcod*.

Modifications must be carried through in library routines:

```
port: CMACHL.inc, ASIMHM.f, GETFD.f, PUTFD.f, GPSGB0.f
gcod: DEGRIB.f, ENGRIB.f
```

tsfs: ASTSFM.f, ASTSFW.f, CPDTRF.f
util: DIASIM.f, DIASTA.f, MANPFD.f

4. Compilation of library *gcod* remains in single precision. This requires that floats in the calling routines to *gcod*-routines are explicitly declared as REAL*4 and that float information in the calling routines is swapped with REAL*8 declared reals prior to invoking the *gcod* -routine, when it is an encrypting calling routine, or after invoking the *gcod* -routine, when it is a decrypting calling routine.

Modifications must be carried through in library-routines:

port: GETFD.f, PUTFD.f, GPSGB0.f
grwl: GREAD.f, GWRITE.f

5. Particularly nasty is the situation where an integer number is passed on in the calling routine, while the receiving routine expects a float. This occurs in the calling of ASTSFW.f from WRITRF.f (both in library *tsfs*). In the calling routine the integer number has been converted into a real.

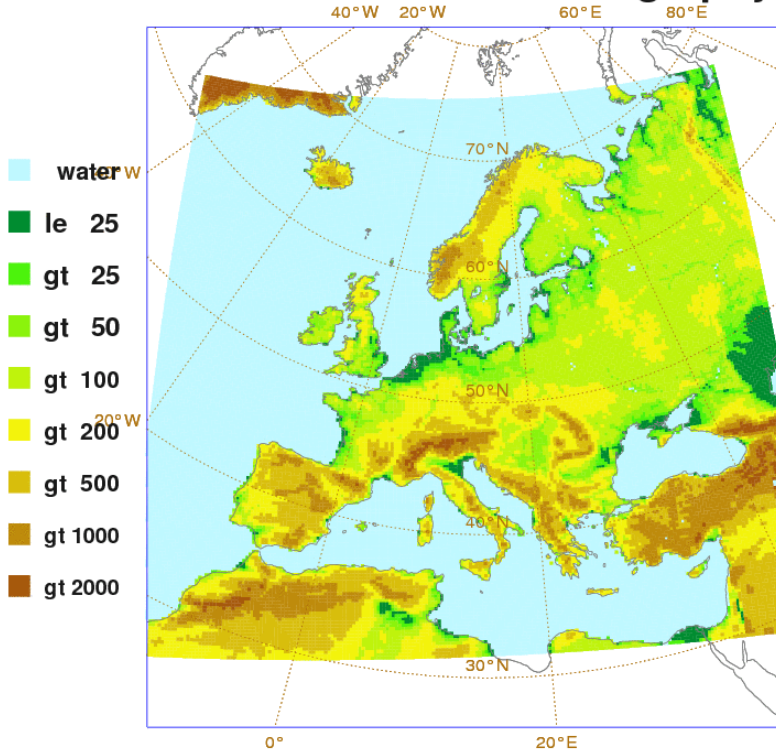
Compiler environment:

1. Code adjustments described above are activated by compiler directive R64I32.
2. Compiler directive FLP_64B must be used instead of FLP_32B.
3. The compiler must be told explicitly that the code should be compiled assuming REAL*8, with the exception of library *gcod*.

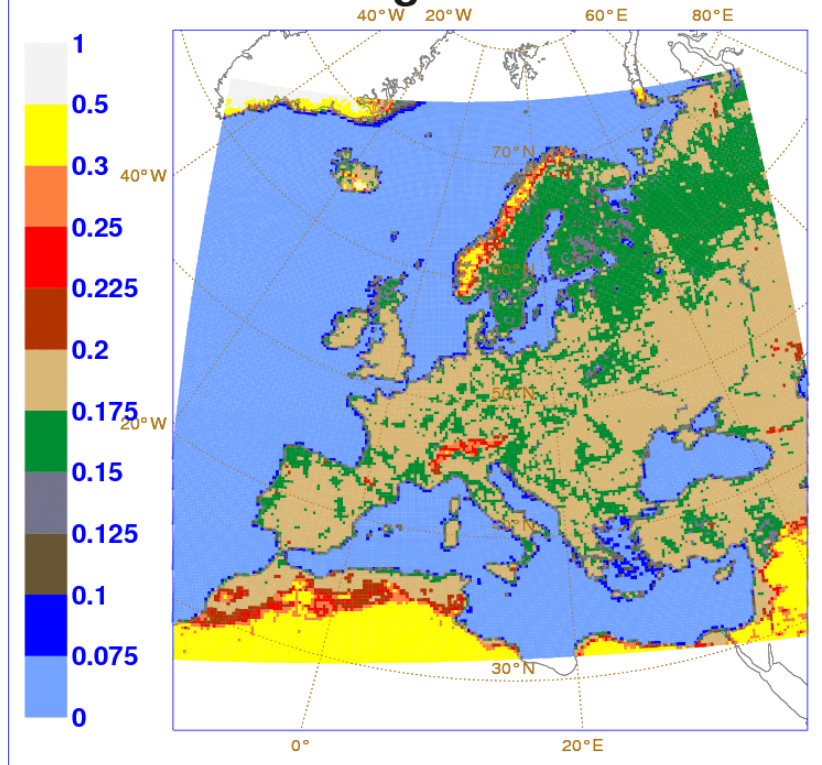
Appendix C: Surface characteristics maps for Europe at 25 km resolution

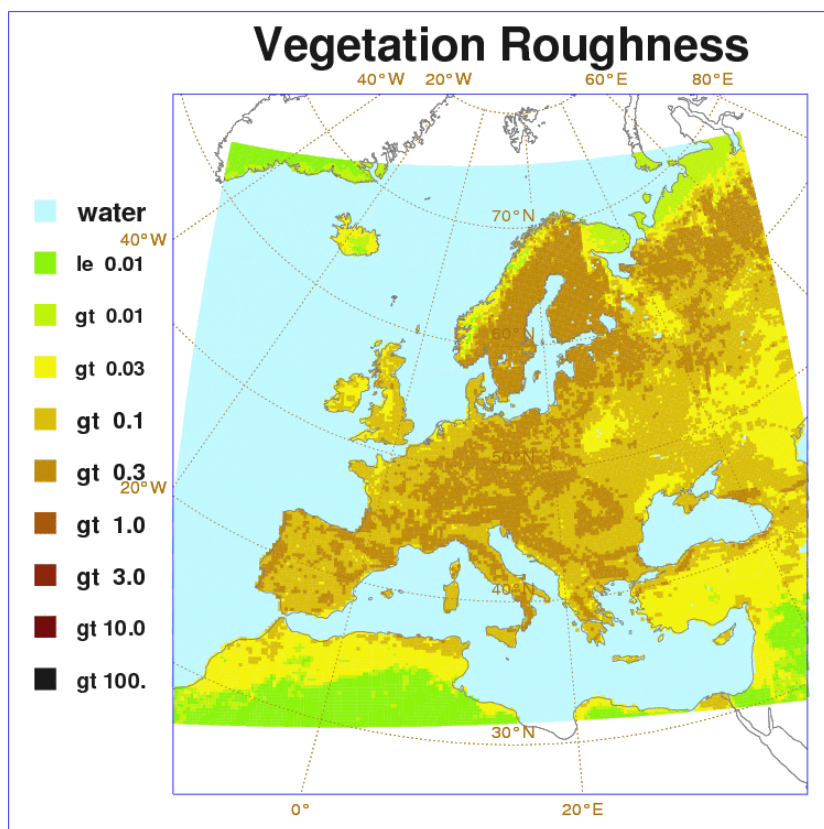
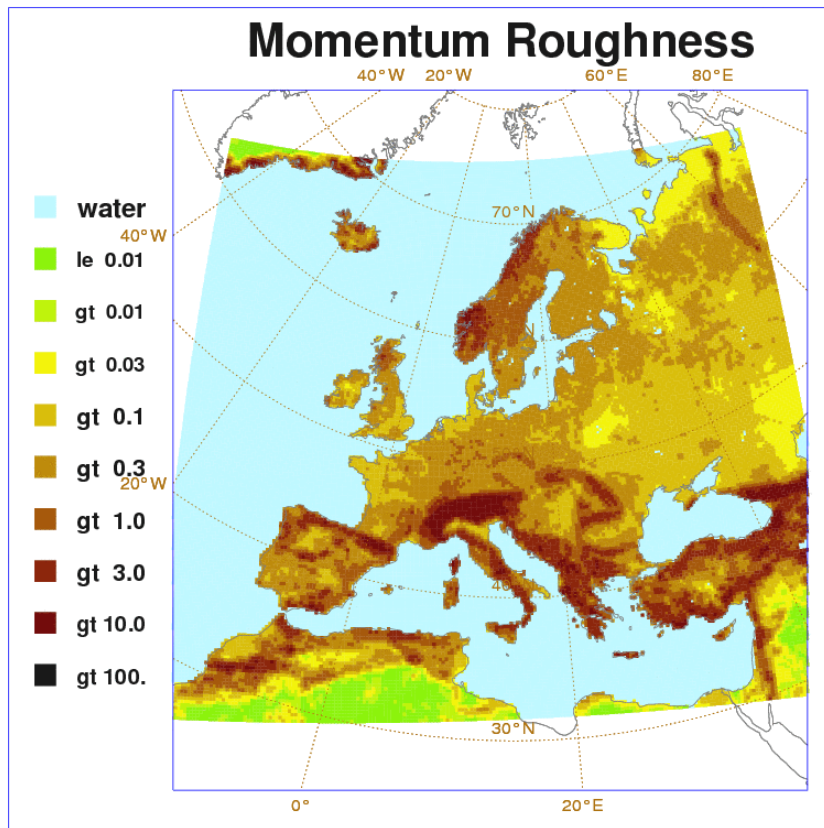
The figures in Appendix C contain European scale maps for the most relevant surface characteristics used by RACMO at 25 km horizontal resolution. Shown are 1) land sea mask and orography, 2) background albedo, 3) momentum roughness length, 4) contribution to the roughness length associated to vegetation, 5) type and 6) fractional cover of high vegetation, 7) type and 8) fractional cover of low vegetation. (The figures for the roughness length parameters, which include a seasonal cycle, refer to the month of September).

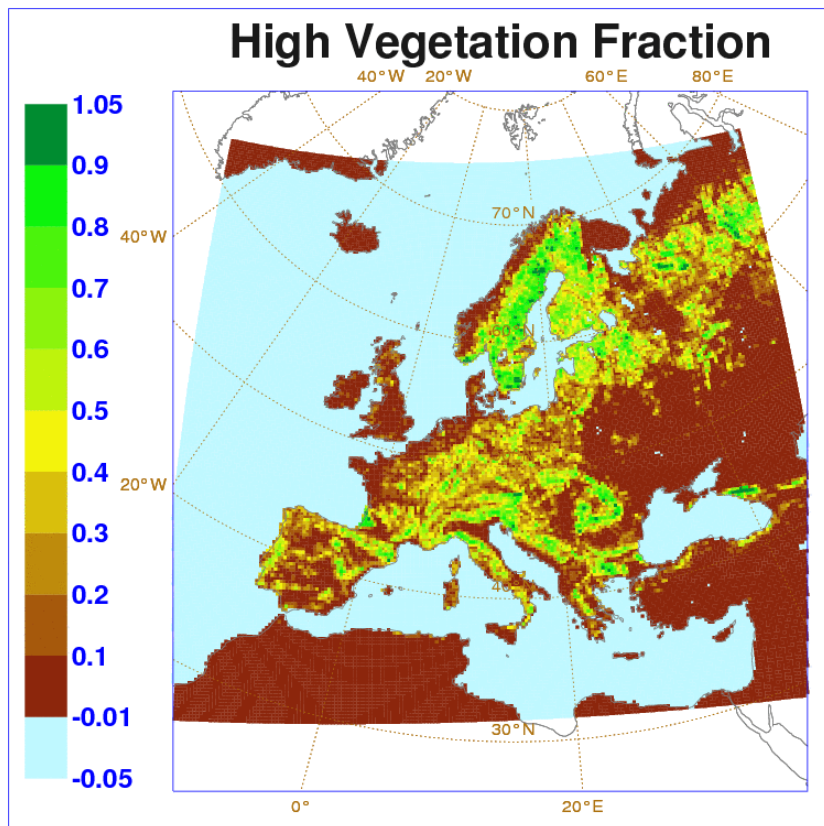
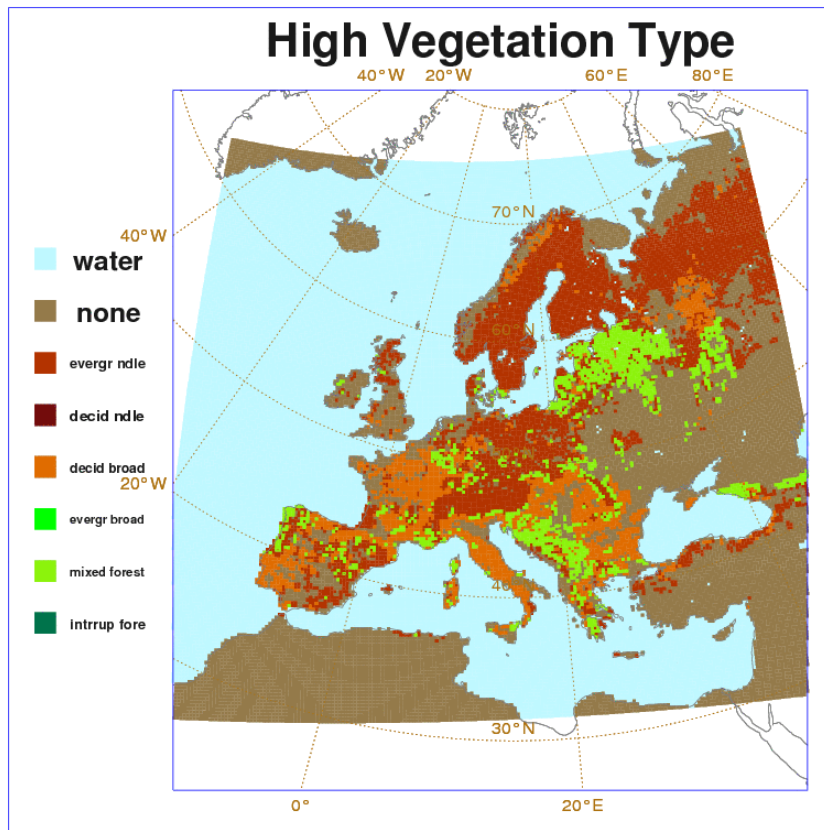
Land Sea Mask and Orography

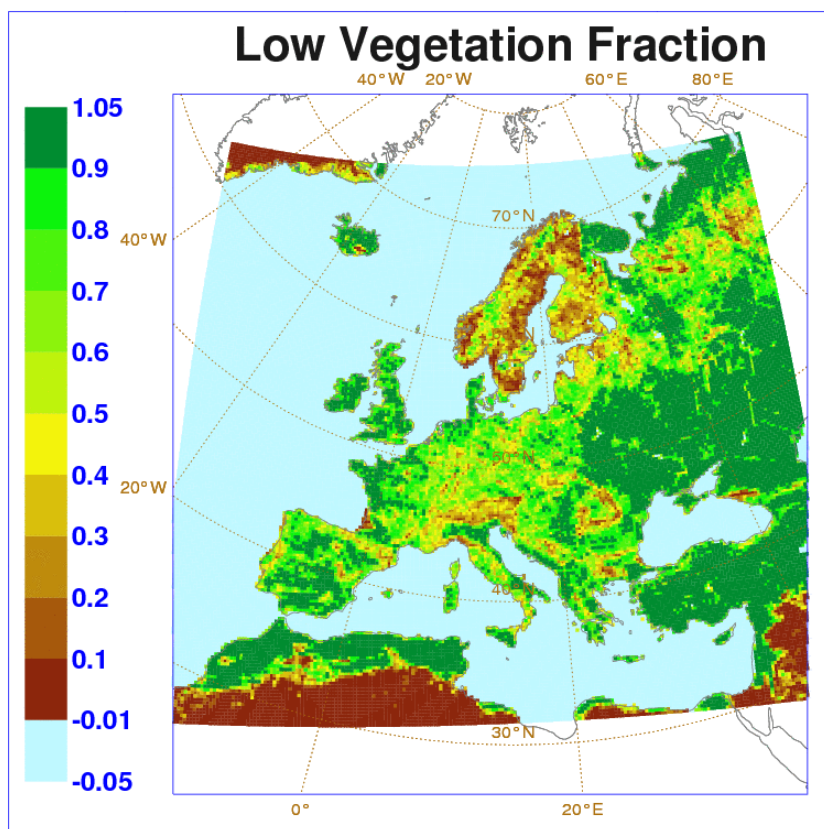
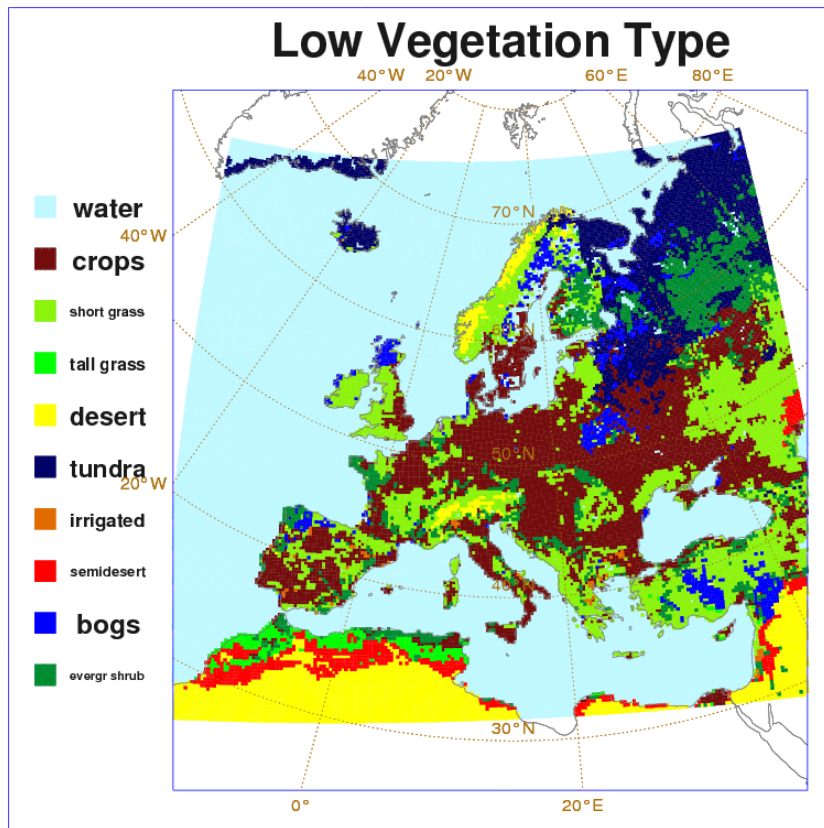


Background Albedo









References

- Beljaars, A.C.M., A.R. Brown, and N. Wood, 2004: A new parameterization of turbulent orographic form drag. *Q.J.R. Meteorol. Soc.*, **130**, 1327-1347
- Bosveld, F.C., E. van Meijgaard, E.I.F. de Bruijn, and G.J. Steeneveld, 2008. The quality of horizontal advective tendencies in atmospheric models. Proceedings 18th AMS workshop on Boundary Layer and Turbulence, 9-13 June 2008, Stockholm, American Meteorological Society.
- de Bruijn, E.I.F., van Meijgaard, E., 2005. Verification of HIRLAM with ECMWF physics compared with HIRLAM reference versions. HIRLAM Technical Report 63, 39pp. Available from SMHI, S-601 76 Norrköping, Sweden.
- Champeaux, J.I., V.Masson and F.Chauvin, 2003: ECOCLIMAP: a global database of land surface parameters at 1 km resolution; *Meteorol. Appl.* **12**, 29-32.
- Donelan, M.A., and co-authors, 2004: On the limiting aerodynamic roughness of the ocean in very strong winds, *Geophys. Res. Lett.*, **31**, L18306, doi: 10.1029/2004GL019460
- Eerola, K., 2004. Testing the Aidan McDonald's modifications. HIRLAM Newsletter **46**, p. 29-32. Available from SMHI, S-601 76 Norrköping, Sweden.
- Ettema, J., M.R. van den Broeke, E. van Meijgaard, W.J. van den Berg, J. Bamber, J. Box, R. Bales, 2008. Surface mass balance of the Greenland ice sheet revealed by high-resolution climate modeling. *Submitted*.
- Holton, J.R., 1979. An introduction to Dynamic Meteorology, Volume 23, 2nd Edition, International Geophysics series (or Volume 88, 2004, 4th Edition), publisher Academic Press
- Jakob, C., A.P. Siebesma, 2003. A new subcloud model for mass-flux convection schemes; Influence on triggering, updraught properties and model climate, *Month Weath. Rev.* **131**, 2765-2778
- Källén, E. (ed.), 1996: HIRLAM Documentation Manual System 2.5, SMHI, Norrköping. Available from SMHI, S-601 76 Norrköping, Sweden.
- Lenderink, G., van den Hurk, B., van Meijgaard, E., van Ulden, A.P., Cuijpers, J., 2003. Simulation of present-day climate in RACMO2: first results and model developments. KNMI Technical Report, 252, 24 pp. Available from KNMI, Postbus 201, 3730 AE, De Bilt, The Netherlands.
- Lenderink, G., E. van Meijgaard, and F. Selten, 2007. Intense coastal rainfall in the Netherlands in response to high sea surface temperatures: analysis of the event of August 2006 from the perspective of a changing climate. *Climate Dynamics*. DOI 10.1007/s00382-008-0366-x

de Martino, G., B. van Ulft, H. ten Brink, M. Schaap, E. van Meijgaard, R. Boers, 2008: An aerosol-cloud module for inclusion in the KNMI regional climate model RACMO2. KNMI Scientific Report, 2008-05, 22 pp. Available from KNMI, Postbus 201, 3730 AE, De Bilt, The Netherlands.

Reijmer, C.H., E. van Meijgaard en M.R. van den Broeke, 2005. Evaluation of temperature and wind over Antarctica in a Regional Atmospheric Climate Model using 1 year of automatic weather station data and upper air observations J. Geophys. Res., 110, 4103, 1-12, doi:10.1029/2004JD005234

Roebeling, R.A., and E. van Meijgaard, 2008. Evaluation of the diurnal cycle of model predicted cloud amount and liquid water path with observations from MSG-SEVIRI, J. Climate, in press.

Rogers, R.R. and M.K. Yau, 1989: A short course in cloud physics, International series in natural philosophy, vol. 113, 3rd ed., Butterworth Heinemann.

Undén, P. et al., 2002: HIRLAM-5 Scientific Documentation, 144 pp. Available from SMHI, S-601 76 Norrköping, Sweden.

White, P.W. (ed.), 2004: IFS documentation CY23r4: Part IV physical processes. <http://www.ecmwf.int/research/ifsdocs/>

Zhang, W., W. Perrie, and W. Li, 2006: Impacts of waves and sea spray on midlatitude storm structure and intensity, Mon. Wea. Rev., 134, 2418-2442

